#### 1

# Monolithically Integrated ε-Ge/In<sub>x</sub>Ga<sub>1-x</sub>As Quantum Well Laser Design: Experimental and Theoretical Investigation

Rutwik Joshi, S. Johnston, S. Karthikeyan, L. F. Lester, *Fellow*, IEEE, and M. K. Hudait, *Senior Member*, *IEEE* 

Abstract— Here, we have analyzed the electrical and optical phenomenon occurring in a ε-Ge/In<sub>x</sub>Ga<sub>1-x</sub>As quantum well (QW) laser through self-consistent physical solvers calibrated using inexperimental results.  $\mathbf{A}$ separate heterostructure QW design is proposed to enable lasing from tensile strained germanium (ε-Ge) in the range of 1.55 μm to 4 μm wavelength as a function of QW thickness and indium (In) composition. Different recombination mechanisms were analyzed as a function of tensile strain in ε-Ge QW. Minority carrier lifetime and band alignment are key attributes of a QW laser, which were measured using microwave photoconductive decay and x-ray photoelectron spectroscopy (as a function of In composition), respectively. The transition point of Ge to a direct bandgap material is re-affirmed to be at  $\varepsilon = 1.6 \%$  (In  $\sim 24 \%$ ) and the transition from type I to type II for ε-Ge/In<sub>x</sub>Ga<sub>1-x</sub>As QW is found to be at In  $\sim$  55 %. Also, the transition to a TM mode dominant laser is identified at In ~ 15 %. Using a tunable waveguide design to optimize confinement as a function of In composition, strain, wavelength, QW thickness, refractive index, and geometry, the ε-Ge QW laser design provided a net material gain of ~ 2000 cm<sup>-1</sup> and a threshold current density of ~ 5 kA/cm<sup>2</sup>, which is an improvement over existing Ge based lasers. The impact of In composition and QW thickness on the band structure, polarized gain spectra, and various lasing metrics were analyzed to show &-Ge/InGaAs QW lasers as promising for integrated photonics.

*Index Terms*— Quantum well laser, Tensile strained Germanium, InGaAs, monolithically integrated light source.

## I. INTRODUCTION

Beyond the age of electronic transistor technology, the future of computing and communication is possible through quantum technologies and photonics. These technologies are presently faced with some key challenges two of which are related to electronic-photonic monolithic integration and interfacing, and silicon (Si) compatibility of multi-material technologies for scaled production. At the center of quantum computation, sensing and photonics lies an electrically powered coherent light source, and the ability to integrate such a light source with Si-compatible technologies on a chip has long been sought [1-3]. Tensile strained germanium ( $\varepsilon$ -Ge) is a potential candidate for such a coherent light source for several reasons:

Manuscript received August 1, 2023. The review of this paper was arranged by Editor xxxxx. Authors acknowledge partial support from the NSF under grant number ECCS- 2042079, a US-Ireland joint R&D program.

Rutwik Joshi, Sengunthar Karthikeyan, L. F. Lester and M. K. Hudait are with the Bradley Department of Electrical and Computer Engineering, Virginia Polytechnic Institute and State University, Blacksburg, VA 24061, USA (mantu@vt.edu).

Steve Johnston is with the National Renewable Energy Laboratory, Golden, Colorado 80401, USA

Digital Object Identifier.

(i) the direct bandgap of Ge could provide ~ 1550 nm wavelength resulting in better compatibility with existing Si photonics and optical communication platforms [3,4], (ii) strain induced tunable bandgap Ge [2,5], (iii) compatibility with modern Si-based electronics fabrication infrastructure, and (iv) ability to form high-performance electronics [5] to drive the light source and interface with external circuitry. The benefits of the rapidly growing quantum technologies can be leveraged, provided a wide range of quantum elements made from different materials and systems can be co-integrated to form a heterogeneous chiplet-based system for achieving quantum supremacy [1]. Such a heterogeneous integration is a major challenge, and the complexity and cost of the process and system can be reduced significantly if the individual elements are compatible with existing Si infrastructure. This monolithically integrated Ge-based laser tunable in the 1.55-4µm range can find a wide set of applications such as: day-time quantum key distribution [6,7], resolving capacity crunch moving to 2-4 µm for fiber communication spectrum [8], reduced linear and nonlinear losses [9] for integrated Si optics, quantum metrology, and sensing [10,11], direct probing of the fundamental absorption bands of nearly all gas molecules [12].

The direct growth of Ge on Si, although an attractive solution for large-scale manufacturing, suffers from a large lattice mismatch (~ 4 %), resulting in defects and dislocations during epitaxial growth [13]. This degradation in epitaxial Ge material quality can be inferred from the minority carrier recombination lifetime measured through microwave reflection photoconductive decay (µ-PCD) method [14]. A higher carrier lifetime is an essential attribute of a bulk or quantum well light source, as it determines the efficiency of electrical conversion as well as the performance of the laser [14,15]. The primary hurdle in the development of an efficient on-chip Ge-based light source is the material quality, i.e., the minority carrier lifetime [15]. The GaAs-based material system (i.e., using In<sub>x</sub>Ga<sub>1-x</sub>As and In<sub>x</sub>Al<sub>1-x</sub>As based intermediary buffers/barriers with GaAs substrate) is a solution for growing high-quality epitaxial Ge for

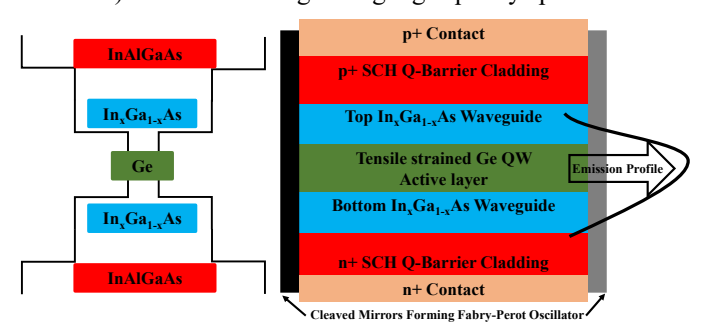


Fig. 1. Schematic of the SCH Ge-on-InGaAs quantum well laser structure and band structure, utilizing pseudomorphic monolithic growth.

two key reasons: (i) lattice match between the epitaxial Ge layer and the GaAs substrate resulting in lower defect density, and (ii) transferability of GaAs based growth and process recipes to large area cost-effective, Si substrate [13].

Apart from material quality, the use of In<sub>x</sub>Ga<sub>1-x</sub>As or In<sub>x</sub>Al<sub>1-</sub> xAs based intermediate buffer can form the waveguide and provide tensile strain in the Ge layer, which can tune the performance and wavelength Ge light source. In this work, we explore the design considerations to develop an efficient and experimentally realizable In<sub>x</sub>Ga<sub>1-x</sub>As/ε-Ge/In<sub>x</sub>Ga<sub>1-x</sub>As quantum well (ε-Ge QW) light source, through structure growth, material characterization, and calibrated TCAD solvers. The minority carrier lifetimes in ε-Ge/In<sub>x</sub>Ga<sub>1-x</sub>As structures are measured through the μ-PCD technique and the band alignment at each ε-Ge/In<sub>x</sub>Ga<sub>1-x</sub>As heterointerface is measured using x-ray photoelectron spectroscopy (XPS) as a function of indium (In) composition. These experimentally determined attributes of a ε-Ge QW laser design such as structure, tensile strain, band alignment, and minority carrier lifetime define the critical design metrics of the laser i.e., emission wavelength, internal quantum efficiency (IQE), threshold current density (J<sub>TH</sub>), power consumption, optical confinement, electrical confinement of the electron and hole wavefunctions, wavefunction overlap, polarization, and maximum optical gain, in an interdependent manner. Here, we isolate the effects of these design parameters on the performance of a ε-Ge QW laser and quantify the design space where Ge can be an efficient coherent light source. The article is organized in the following order: Section II briefly discusses the material growth considerations for ε-Ge/In<sub>x</sub>Ga<sub>1-x</sub>As QW stack shown in Fig. 1, Section III discusses the XPS band alignment measurement and TCAD model calibration along with the impact of In composition on the band structure and band alignment, Section IV describes the measurement of μ-PCD minority carrier lifetime, Section V details the theoretical framework used for the analysis of the waveguide, gain spectra and performance, Section VI details the design and performance metrics of the proposed ε-Ge/In<sub>x</sub>Ga<sub>1-x</sub>As QW as a function of In composition and QW thickness, and Section VII summarizes the recent works on Ge lasers and provides a comparison with the proposed design.

## II. MATERIAL SYSTEM: GROWTH AND STRUCTURE

Compositionally graded buffers that utilize the benefits of metamorphic as well as pseudomorphic growth are of great interest since they offer an approach to bridge the substrate lattice constant to a desired value for device applications such as high electron mobility transistors or QW lasers. The growth of high quality ε-Ge/In<sub>x</sub>Ga<sub>1-x</sub>As OW structures is achieved through vacuum interconnected dual chamber solid source molecular beam epitaxy [16]. A separate confinement layer based on a quaternary alloy, AlGaInAs (cladding layer) is needed for optical confinement while also providing the carriers for injection into the QW. One way to achieve this is to introduce the Al atoms into the InGaAs during material synthesis, forming a quaternary AlGaInAs layer. The choice of the quaternary AlGaInAs composition requires consideration of a key trade-off between growth ease and optical confinement of the emission electric field. Using a higher composition of Al

needs a higher growth temperature and higher Al results in more surface undulations and roughness. Whereas, a higher Al composition would result in a higher bandgap of the quaternary, thus providing a higher refractive index difference with the QW, consequently better optical confinement. However, using a low Al composition reduces the bandgap and refractive index differences between the waveguide core and the cladding, thus reducing the optical confinement. Furthermore, the In composition in the quaternary buffers (Q-buffers) needs to be identical to the In composition in the confinement layer (In<sub>x</sub>Ga<sub>1-x</sub>As) of the QW during MBE growth, thus providing a constraint on the choice of the Q-buffer composition.

The ε-Ge/In<sub>x</sub>Ga<sub>1-x</sub>As QW structure shown in Fig. 1 can be grown on a GaAs substrate followed by a lattice grading In<sub>x</sub>Ga<sub>1</sub>xAs buffer to mitigate the lattice mismatch induced defects and dislocations. The topmost part of the In<sub>x</sub>Ga<sub>1-x</sub>As buffer forms virtually defect-free bottom waveguide layer for the ε-Ge QW structure. The pseudomorphic growth of ε-Ge on In<sub>x</sub>Ga<sub>1-x</sub>As is possible [16], provided the thickness of the ε-Ge epitaxial layer remains below the critical layer thickness [17]. The starting substrate off-cut along with migration enhanced epitaxy using arsenic pre-layer are needed for anti-phase domain free In<sub>x</sub>Ga<sub>1</sub>. <sub>x</sub>As layer on ε-Ge. The AlGaInAs quaternary separate confinement heterostructure (SCH) layer can be grown before the InGaAs bottom waveguide layer with p-type doping and after the InGaAs top waveguide layer with n-type doping, as shown in Fig. 1. Recently, 6 Å interface abruptness of ε-Ge/In<sub>0.24</sub>Ga<sub>0.76</sub>As heterostructure (grown by MBE) was demonstrated by atom probe tomography [16]. Thus, such growth of a multilayer heterostructure, which can form a  $\varepsilon$ -Ge/In<sub>x</sub>Ga<sub>1-x</sub>As QW laser is possible with minimal defects and dislocations in the active region.

## III. $\epsilon$ -Ge/In<sub>x</sub>Ga<sub>1-x</sub>As Band Alignment Calibration and Framework

The band alignment of various In compositions in  $\varepsilon$ -Ge/In<sub>x</sub>Ga<sub>1-x</sub>As heterostructures were constructed using the experimentally determined band offset values measured using the x-ray photoelectron spectroscopy (XPS) on a PHI Quantera SXM-03 (Scanning XPS Microprobe) system, reported in Refs. [18-21]. For the band structure and offsets calibration, the  $30\times30~{\bf k}\cdot{\bf p}$  calculated material and band parameters are adopted from Ref. [22]. The simulations are tuned to utilize a  $6\times6~{\bf k}\cdot{\bf p}$  approximation along with linear deformation theory within Sentaurus TCAD [23] to accurately predict experimental values of band offsets, and  $30\times30~{\bf k}\cdot{\bf p}$  calculations of the band structure of  $\varepsilon$ -Ge/In<sub>x</sub>Ga<sub>1-x</sub>As system. To ensure the accuracy of the electrical predictions, the drift-diffusion and quantum-corrected electrical behavior of the model for nanoscale devices has been calibrated and reported elsewhere [5,24].

Fig. 2(a) shows the experimentally measured and simulated valence band offsets ( $\Delta E_v$ ) of  $\epsilon$ -Ge/In<sub>x</sub>Ga<sub>1-x</sub>As heterostructures as a function of In composition in the In<sub>x</sub>Ga<sub>1-x</sub>As layer. The solid circle represents the experimental data and the solid line is the simulated data, and an excellent agreement can be seen between the experimental and modeled band offsets. In addition, using the measured value of  $\Delta E_v$  and bandgap values of both  $\epsilon$ -Ge as well as In<sub>x</sub>Ga<sub>1-x</sub>As via 30×30  $\mathbf{k} \cdot \mathbf{p}$  [2], the conduction band offsets ( $\Delta E_c$ ) are evaluated. Due to the two

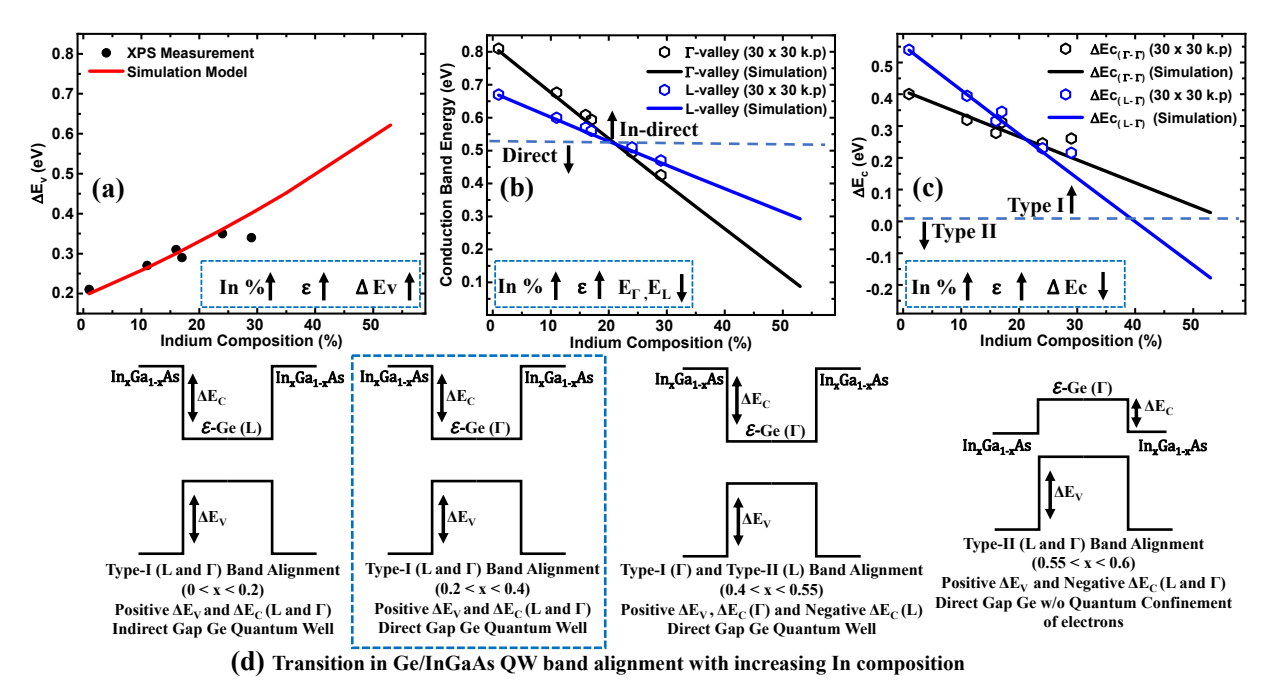


Fig. 2.  $\epsilon$ -Ge/In<sub>x</sub>Ga<sub>1-x</sub>As system band alignment using XPS and model calibration as a function of In composition and tensile strain: (a) Valence band offset ( $\Delta E_v$ ) (b)  $\Gamma$ - and L-valley energies showing the transition from indirect bandgap to direct bandgap Ge, (c) Conduction band offset ( $\Delta E_v$ ) showing the transition from Type I to Type II, and (d) schematic for alignment configurations and transition of the  $\Gamma$ - and L-valley of the Ge/InGaAs QW.

conduction band minima (L- and  $\Gamma$ -valley), one can construct  $\Delta E_c$  using  $\Gamma$ -valley of  $In_xGa_{1-x}As$  ( $\Gamma$ -valley dominates for any In composition) and either L-valley or  $\Gamma$ -valley of Ge depending on the strain present within the  $\varepsilon$ -Ge layer (via In<sub>x</sub>Ga<sub>1-x</sub>As strain template). Fig. 2(b) shows the conduction band energy of  $\varepsilon$ -Ge due to L-and  $\Gamma$ -valley as a function of In compositions by 30×30 k·p and TCAD simulation model [23]. In this figure, the open circle is the data obtained from 30×30  $\mathbf{k} \cdot \mathbf{p}$  for both L-and  $\Gamma$ -valley, and the solid line represents the simulated data. The indirect-to-direct bandgap transition takes place  $\sim 24\%$  In ( $\varepsilon = 1.6\%$ ), reaffirming the finding reported in Ref. [2,25]. Fig. 2(c) shows the  $\Delta E_c$  using the bandgaps of  $\epsilon$ -Ge (Fig. 2b) and In<sub>x</sub>Ga<sub>1-x</sub>As as a function of In composition between the L-and  $\Gamma$ -valley of  $\epsilon$ -Ge and  $\Gamma$ -valley of  $In_xGa_{1-x}As$ . The open circle is the data obtained from  $30\times30$  k·p and solid lines from the simulated results fitted to the 30×30 k·p data. In all cases, there is an excellent agreement between the experimental (Fig. 2a) and the simulated results.

Fig. 2 shows that as the In composition increases in the  $In_xGa_{1-x}As$  layer, the tensile strain in the Ge QW increases resulting in (i) a decrease in Γ-valley of Ge at a rate of  $13.24 \frac{meV}{ln\%}$  or  $196.02 \frac{meV}{ε\%}$ , and (ii) a decrease in L-valley of Ge at a rate of  $6.89 \frac{meV}{ln\%}$  or  $102.02 \frac{meV}{ε\%}$ . Furthermore, the tensile strain results in a broken degeneracy between light hole (LH) and heavy hole (HH) valence bands, while moving the LH band upwards. It is important to note that radiative transitions are possible from the LH as well as the HH bands, and the carriers participating in these transitions will experience different band offsets as well as different transition energies, optical polarization, and gain. Fig. 2(d) shows the different band alignment configurations for  $In_xGa_{1-x}As/ε$ -Ge/ $In_xGa_{1-x}As$  QW configuration as a function of In compositions. Here, we assume symmetric heterointerface band alignment remains type

I up to 40 % In composition for L-valley and 55 % In composition for  $\Gamma$ -valley. For In compositions 0.4 < x < 0.55 range, the band alignment is type I with  $\Gamma$ -valley of  $\epsilon$ -Ge (the band alignment is Type-II for the L-valley of  $\epsilon$ -Ge) thus ensuring acceptable direct bandgap QW confinement up to In composition of  $\sim$  55 %. The system transitions to a type II alignment for both L- and  $\Gamma$ -valleys beyond an In composition of  $\sim$  55 %. The bandgap of  $\epsilon$ -Ge drops significantly for high tensile strain and beyond an In composition of 60 %, the Ge bandgap is negative. It can also be seen from Fig. 2(d) that the  $\epsilon$ -Ge/In<sub>x</sub>Ga<sub>1-x</sub>As QW system will remain type I for the majority of the In compositions (0 - 55 %) and completely type II for a short range (55 - 60%). This ensures that the  $\epsilon$ -Ge QW provides carrier confinement and has the potential to be a tunable light source over a wide range of wavelengths.

XPS measurements provide information about the valence band maximum (VBM), which is always aligned with the LH band for all strain configurations [2] studied here, thus the offsets and energies shown in Fig. 2 are corresponding to the LH band. The HH-band energies and offsets can be calculated as a function of In composition or strain relative to the LH band as follows [2],  $E_{VBM,HH} = E_{VBM,LH} - (8.66 \text{ meV} \times In \%)$ . Due to the difference in the behavior of the LH and HH bands with applied tensile strain, the carriers in the HH band experience a small and constant valance band offset in the range of 0.15 - 0.19 eV, unlike the LH band which can be seen to vary considerably in Fig. 2(a). Due to the faster reduction rate of the Γ-valley compared to the L-valley with increasing In composition, Ge transitions to a direct bandgap active material at In composition of ~ 24 % and corresponding tensile strain of  $\sim 1.6 \%$  [2, 25]. In the  $\varepsilon$ -Ge QW laser, the band alignment between the ε-Ge active layer and the In<sub>x</sub>Ga<sub>1-x</sub>As waveguide layer, determines the extent of quantum confinement of both electrons and holes. This also affects the overlap between the electron and hole wavefunctions as well as wavefunction

spillage outside the QW for higher In compositions. Furthermore, as Ge transitions from an indirect bandgap material to a direct bandgap material, the band alignment also gradually changes, as seen in Fig. 2. The  $\Delta E_V$  determines the confinement of holes in the  $\varepsilon$ -Ge active layer, and it is measured to be always positive (see, Fig. 2a), indicating that hole bound states will exist for all In compositions and corresponding tensile strains in Ge. Due to the significantly higher density-ofstates (DOS) in the Ge L-valley ( $\sim 50 \times$ ) compared to the  $\Gamma$ valley [2], the carrier occupations in the L-valley are dominant even after Ge transitions to a direct bandgap lasing medium. Thus, the band alignment associated with the L- and  $\Gamma$ -valley needs to be considered simultaneously as shown in Fig. 2(c) to understand the complete 3D electrical behavior of the  $\varepsilon$ -Ge OW laser. However, radiative transitions are only possible from the  $\Gamma$ -valley since the L-valley transition probability is extremely low, contributing negligible gain [26].

## IV. CARRIER LIFETIME BY μ-PCD

The prediction of  $\varepsilon$ -Ge/In<sub>x</sub>Ga<sub>1-x</sub>As QW laser performance requires an assessment of Ge active layer material quality, to qualitatively affirm low defects and dislocations. In the present work, the carrier lifetime of  $\sim 0.7\%$   $\varepsilon$ -Ge/In<sub>0.11</sub>Ga<sub>0.89</sub>As heterostructure 1500 nm laser wavelength was evaluated using microwave photoconductive decay ( $\mu$ -PCD) measurement technique, shown in Fig. 3. The estimated injected carrier density is approximately  $10^{13}$  cm<sup>-3</sup> and the excitation power was  $\sim 2$  mW, details of  $\mu$ -PCD measurement technique can be found in Ref. [27]. The minority carrier recombination lifetime of 81 ns for 0.7 %  $\varepsilon$ -Ge due to Shockley-Read-Hall (SRH) recombination was determined by fitting the  $\mu$ -PCD decay curve. This PCD lifetime value for the SRH recombination, as well as other non-radiative recombination mechanisms such as Auger processes, are included in the calibrated model.

## V. LASER PERFORMANCE: OPTICAL GAIN, THRESHOLD, AND QUANTUM EFFICIENCY

The carrier lifetime (Fig. 3) and the band alignment (Fig. 2) for tunable  $\varepsilon$ -Ge/In<sub>x</sub>Ga<sub>1-x</sub>As systems are provided as input to the TCAD simulation suite [23]. This simulation framework considers a 3D numerical solver accounting for the drift-diffusion and quantum-corrected physics within the  $\varepsilon$ -Ge/In<sub>x</sub>Ga<sub>1-x</sub>As QW structure. The model includes experimentally calibrated band offsets considering multivalley band structure (Fig. 2) and accounts for composition, strain,

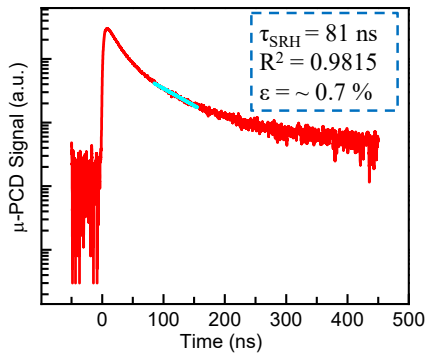


Fig. 3. Minority carrier lifetime measured using  $\mu$ -PCD technique along with the curve fitting for tensile strained Ge of 0.7 % (Ge/InGaAs at In = 11 %).

electric field, non-parabolicity, doping-dependent band structure, mobility, and effective mass. The electrical parameters such as electrostatic potential, quasi-fermi energy levels, current and voltage, recombination rates (SRH, Auger, and Radiative), band occupations, wavefunctions, and  $6\times6$  **k·p** band structure are self-consistently solved [23] to calculate the optical gain spectra. The model also accounts for the thermionic emission rates over the heterointerfaces and a high ( $5\times10^{12}$  cm<sup>-2</sup>V<sup>-1</sup>) interface trap density at the two  $\varepsilon$ -Ge/In<sub>x</sub>Ga<sub>1-x</sub>As heterointerfaces to ensure a more realistic electrostatic profile in the  $\varepsilon$ -Ge QW. The electrical parameters listed above are fed to TCAD laser-gain solver to calculate the optical gain of the  $\varepsilon$ -Ge/In<sub>x</sub>Ga<sub>1-x</sub>As finite QW laser structure [28-30].

## A. Optimum Waveguide Design: Optical confinement factor

The confinement of the optical mode depends on the refractive index difference between the AlGaInAs SCH cladding, InGaAs waveguide, and ε-Ge QW active region as well as the emission wavelength (function of In composition), geometry, and composition. The optimal optical confinement factor ( $\Gamma_{ont}$ , not to be confused with the  $\Gamma$ -valley, discussed above) is calculated considering a step refractive index with In<sub>x</sub>Ga<sub>1-x</sub>As waveguide core and (AlGa)<sub>1-x</sub>In<sub>x</sub>As SCH Q-barrier (refractive index is assumed to be 3.1) as the cladding. The refractive index  $(n_1)$  and bandgap of the  $In_xGa_{1-x}As$  waveguide core are calculated according to the Sellmeier equation [31], where the lasing wavelength is obtained from the gain spectrum of the ε-Ge QW laser. The optical confinement factor ( $\Gamma_{opt}$ ) is calculated assuming a 3-layer symmetric waveguide confining the mode as shown schematically in Fig. 1, forming the characteristic equation given by [28],  $k_z \tan(\frac{k_z d}{2}) = \gamma$  where

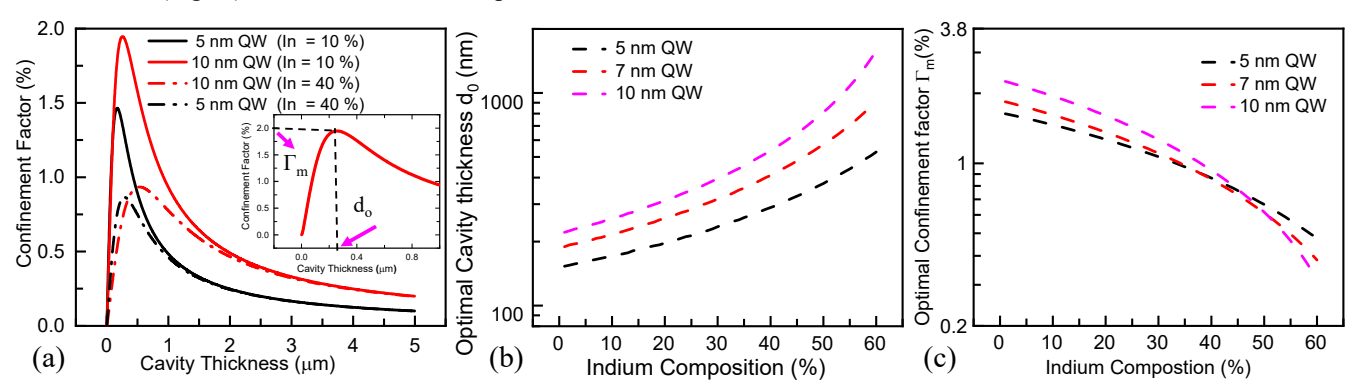


Fig. 4. Design of optimum SCH Ge/InGaAs QW cavity: (a) Impact of In composition, QW and cavity thickness on the optical confinement. Variation of (b) optimal cavity thickness  $d_{\theta}$  and, (c) optimal confinement factor  $\Gamma_{m}$  with In composition, used in calculations of laser performance.

 $k_z$  is the propagation constant in the active region along the growth direction (z-axis), d is the total thickness of the  $In_xGa_{1-x}As$  waveguide,  $\gamma$  is the propagation constant for the cladding Q-barrier layer (AlGaInAs) with  $k_z^2 + \gamma^2 = k_0^2 (n_1^2 - n_2^2)$  and  $k_0$  as the free space wave-number. The fraction of the electric field contained in the central slab of the waveguide can be calculated using the relation [28],

$$\Gamma_{opt} = \frac{\int_{-d/2}^{d/2} |E(x,z)|^2 dz}{\int_{-\infty}^{\infty} |E(x,z)|^2 dz} = \frac{1 + (2\gamma d/V^2)}{1 + (2/\gamma d)},\tag{1}$$

where,  $V=k_0d\sqrt{{n_1}^2-{n_2}^2}$  is the normalized frequency and  $n_2$  is the refractive index of the AlGaInAs SCH Q-barrier layer. The Ge QW thicknesses in the 5 - 20 nm range confined inside the In<sub>x</sub>Ga<sub>1-x</sub>As waveguide face an inverse relation for the optical confinement [30]. The optimum  $\Gamma_{opt}$  can be found by maximizing these transcendental relations using iterative solutions. In addition, the overlap of the optical energy distribution with the QW needs to be maximized within the waveguide to obtain the maximum confinement factor  $(\Gamma_m)$ . This confinement maxima ( $\Gamma_{\rm m}$ ) depends on the wavelength of emission, step-graded refractive index, QW thickness, and the thickness of the SCH layer. As the In composition in the waveguide is increased, the tensile strain in Ge and correspondingly the emission wavelength ( $\lambda_e$ ) increases. Thus, the optimal waveguide design for different In composition and ε-Ge QW thickness is shown in Fig. 4(a), indicating that for a particular In composition and ε-Ge QW thickness, there exists an optimal waveguide thickness  $d_0$  where the  $\Gamma_{opt}$  is optimal  $(\Gamma_{\rm m})$ . The variation of  $d_0$  and  $\Gamma_{\rm m}$  with In composition is shown in Fig. 4(b) and (c). Optical confinement factors are expected to be nearly identical for the TE and TM modes for a fixed emission wavelength [29]. But in the proposed ε-Ge/In<sub>x</sub>Ga<sub>1-x</sub>As QW laser structure, the  $\Gamma_{opt}$  for the TE and TM modes would vary marginally depending on the emission wavelength of the LH and HH transitions, and correspondingly affect the gain and threshold performance.

The results shown in Fig. 4, the waveguide cavity thickness, *i.e.*, the  $In_xGa_{1-x}As$  layer thickness on either side of the  $\varepsilon$ -Ge QW is fixed at the optimum value  $d_0/2$  depending on the QW thickness and In composition. This approach is well-suited for the gain and threshold predictions, where the  $\Gamma_{opt}$  for any design combination is ensured to be maximum. For certain regions in Fig. 4(c) (*e.g.*, at In = 20-40%), one can notice that the dependence of  $\Gamma_m$  ( $\Gamma_{opt}$ ) on the QW thickness is nearly eliminated. At these In compositions, one can move to a thinner QW and benefit from the higher material gain G (as well as modal gain g) without paying a penalty with the optical confinement, as will be seen in the following sections. This is an advantage of the tunable design methodology selected here, where the laser stack is designed to optimize the confinement of the mode.

## B. Material gain and transition matrix elements

Electrons from the  $\Gamma$ -valley can radiatively recombine with holes from the LH and HH band in the  $\epsilon$ -Ge QW. Furthermore, quantization of the bands creates discrete sub-bands in all bands, resulting in radiative transitions from each of them

following Fermi's Golden rule [28]. Due to the higher  $\Delta E_c$  and  $\Delta E_v$ , at least 1 quantized level can be bound in the  $\varepsilon$ -Ge finite QW even at room temperature for most of the strain range. These radiative transitions are classified as the ground state transitions (A:  $\lambda_{pk(\Gamma^1\text{-LH}^1)}$ , B:  $\lambda_{pk(\Gamma^1\text{-HH}^1)}$ ) and the first excited state transitions (C:  $\lambda_{pk(\Gamma^2\text{-LH}^2)}$ , D:  $\lambda_{pk(\Gamma^2\text{-HH}^2)}$ ). Each of these transitions show distinct lasing gain spectra and threshold performance, shown below, with the ground state transitions being the most dominant transition. The material gain, G (where modal gain,  $g = G\Gamma_{opt}$ ) [30] of the  $\varepsilon$ -Ge QW is calculated as a function of emitted photon energies [30],

$$G(E_p) = \int \sum_{j=LH,HH} \sum_{n} DOS_r(E,j,n) \cdot A(j,n)$$

$$\cdot \left(F_{c,n,j}(E) - F_{v,n,j}(E)\right)$$

$$\cdot \frac{\left(\frac{h}{2\pi\tau_{in}}\right)^2}{\left(\frac{h}{2\pi\tau_{in}}\right)^2 + \left(E_p - E\right)^2} \cdot dE$$
(2)

where, j is the index associated with the valence bands LH and HH, n is the number of sub-bands formed in the QW,  $E_{cn}$  and  $E_{vn}$  are eigen energies of the  $n^{th}$  eigenstates for the  $\epsilon$ -Ge QW with In composition dependent finite band offsets (see, Fig. 2).  $DOS_r(E,j,n)$  is the reduced density of states for the conduction and valence bands for each of the sub-bands. The Lorentzian broadening is considered with an intra-band relaxation time of  $\tau_{in} = 0.1 \ ps$  [30]. The transition probability is A(j,n) [30],

$$A(j,n) = \frac{q\pi^2 h}{c \, m_0 \, \epsilon_0 \, n_{Ge} \, E_{tr,n}} \left| M_{T,qw} \left( E_{tr,n} \right) \right|^2, \tag{3}$$

where, h is the Plank's constant, q is the charge of the electron, c is the speed of light,  $m_0$  is the electron mass,  $\epsilon_0$  is the free space permittivity,  $n_{Ge}$  is the refractive index, and the transition matrix element  $\left|M_{T,qw}(E_{tr,n})\right|$  is a function of transition energy, wavefunction overlap and polarization for the  $\epsilon$ -Ge QW [28]. Note that A(j,n) for the  $\epsilon$ -Ge QW would vary significantly as the tensile strain is varied from 0 - 3% due to the drastic changes in the Ge band-structure. Thus, A(j,n) in the above material gain has been moved inside the summation operation to account for a unique A(j,n) associated with each transition.

The polarization (TE vs TM) dependence of transitions can be understood using the relative transition strength associated with the two interacting eigenstates and their corresponding wavefunctions. This relative transition strength is defined as the ratio of the transition matrix element and the momentum matrix element  $\frac{|M_T|^2}{|M_0|^2}$ . Consequently, this ratio will determine the relative transition probability of various transitions between sub-bands under consideration [29]. In the  $\varepsilon$ -Ge/InGaAs QW laser design, the degeneracy between LH and HH bands is broken due to the biaxial tensile strain, and transitions from their corresponding sub-bands would be competing for gain while also resulting in different polarizations (TE or TM) of light. Also, the cavity will support many other modes, and the accurate optical polarization would be quasi-TE or quasi-TM, here the analysis is done for the fundamental mode. In the case

of bulk Ge lasing medium, the Γ-LH and Γ-HH relative transition strength would be equal for the TE and TM modes. But in QW structures, this relative transition probability is redistributed between TE and TM modes unequally, the Γ-LH transition would only contribute to the material gain of the TM mode ( $G_{TM}$ ) and the Γ-HH transition would contribute largely to the material gain of the TE mode ( $G_{TE}$ ). The calculation of these transition matrix elements (between  $n^{th}$  sub-bands following k-selection) proceeds through the calculation of the overlap integrals between the interacting wavefunctions in the finite QW given by [29],

$$|M_T|^2 = |M_0|^2 \left\{ \frac{2}{3} \left| \left\langle \psi_{\Gamma, n} \left| \psi_{LH, n} \right\rangle \right|^2 \right\}, \text{ for TM mode}$$
 (4)

$$|M_T|^2 = |M_0|^2 \left\{ \frac{1}{6} \left| \left\langle \psi_{\Gamma,n} \left| \psi_{LH,n} \right\rangle \right|^2 + \frac{1}{2} \left| \left\langle \psi_{\Gamma,n} \left| \psi_{HH,n} \right\rangle \right|^2 \right\} \right\}, \text{ for TE mode}$$
 (5)

where,  $\psi_{\Gamma,n}$  is the normalized wavefunction of the  $n^{th}$  sub-band electron in the  $\Gamma$ -valley,  $\psi_{LH,n}$  and  $\psi_{HH,n}$  are the normalized wavefunctions of the  $n^{th}$  sub-band holes in the LH and HH band, respectively. Thus, with the application of tensile strain distinct considerations of gain and optical confinement for the various transitions and corresponding TE and TM polarization of the output are required to determine which transitions ultimately lase. The momentum matrix element  $|M_0|^2$  is determined through the modified expression for each transition [29],

$$|M_0|^2 = \left(m_0 E_g/2\right) \left(\frac{m_0}{m_{eff,e}} - 1\right) \left(\frac{E_{tr,n} + so}{E_{tr,n} + \left(\frac{2}{3}\right) so}\right)$$
 (6)

where,  $m_{eff,e}$  is the effective mass of the electron in the conduction band and so is the energy of the spin-orbit VB energy assumed to be 0.29 eV for Ge.

## C. $\varepsilon$ -Ge/In<sub>x</sub>Ga<sub>1-x</sub>As QW gain spectrum

The material gain (G) spectrum is computed in the broad range of energy from 0.3 - 1.2 eV to resolve any features associated with at least 4 major peaks (labeled as A, B, C, D), and their movement with increasing tensile strain and QW thickness. The injection of carriers by pumping needed to overcome losses such as, mirror loss of the Fabry-Perot cleaved facets and free carrier absorption (FCA) are quantified through threshold current density (J<sub>TH</sub>) and carrier density (N<sub>TH</sub>). At the

injection level of  $J_{TH}$  (correspondingly  $N_{TH}$ ), the modal gain greaches threshold and is equal to the total losses, i.e.,  $g = g_{th} =$  $\alpha_{tot}$ . Here,  $\alpha_{tot} = \alpha_{fca}\Gamma_{opt} + \alpha_m + \alpha_{others}$ , is the total loss associated with the ε-Ge QW laser structure. The laser-gain solver calculates the net material gain (G<sub>net</sub>) beyond all material losses, considering three main sources of loss: FCA ( $\alpha_{fca}$ ), optical confinement loss due to the narrow QW and the mirror loss  $(\alpha_m)$  due to the cleaved Fabry-Perot oscillator mirrors. The dominant source of modal loss in a QW is  $\alpha_m$  since the small  $\Gamma_{opt}$  scales the  $\alpha_{fca}$  making it a lesser concern. Unfortunately, due to the higher emission wavelengths attributed to the high tensile strains in Ge, the FCA is expected to increase. But the drastically lower J<sub>TH</sub>/J<sub>TR</sub> and N<sub>TH</sub>/N<sub>TR</sub> associated with these low band bandgap materials, as well as the low doping will reduce the FCA. Hence, to simplify the analysis, considering the large variation in reported FCA values for ε-Ge laser structures, we have assumed a constant and high FCA of 500 cm<sup>-1</sup> [22] [26,32-34]. The proposed ε-Ge/In<sub>x</sub>Ga<sub>1-x</sub>As QW laser structure can provide considerable net gain even if the FCA is an order of magnitude larger than expected. Note that at the wavelength of operation, the FCA associated with InGaAs waveguide and Qbarrier is expected to be orders of magnitude lower than Ge.

Beyond the threshold condition for overcoming all the losses listed above, additional pumping will result in additional gain which eventually saturates at a value identified as the maximum material gain  $G_{\text{max}}$ . The internal quantum efficiency (IQE or  $\eta_i$ ) is the ratio of radiative recombination rate to the total recombination in the  $\varepsilon$ -Ge QW laser structure at maximum gain,  $\eta_i = \frac{J_{rad}}{J_{rad} + J_{non-rad}}$ , where  $J_{non-rad}$  includes the non-radiative recombination mechanisms such as SRH and Auger recombination [23], both of which are dependent on the band structure, minority carrier lifetime, and injection density.

#### VI. RESULTS AND DISCUSSIONS

In this section, the electrical and optical performance metrics as well as the physical design considerations of the  $\varepsilon\textsc{-}\mbox{Ge/In}_x\mbox{Ga}_{1\textsc{-}x}\mbox{As}$  QW laser structure (shown in Fig. 1) are discussed. The cavity is designed at the optimum value of  $d_0$  and  $\Gamma_m$ , as discussed in Fig. 4. The proposed  $\epsilon\textsc{-}\mbox{Ge/In}_x\mbox{Ga}_{1\textsc{-}x}\mbox{As}$  QW laser has potential to utilize a low doped  $\epsilon\textsc{-}\mbox{Ge}$  active layer with moderate-to-high tensile strain and obtain efficient lasing at  $J_{TH}$  well below  $10~k\mbox{A/cm}^2$ , as discussed below.

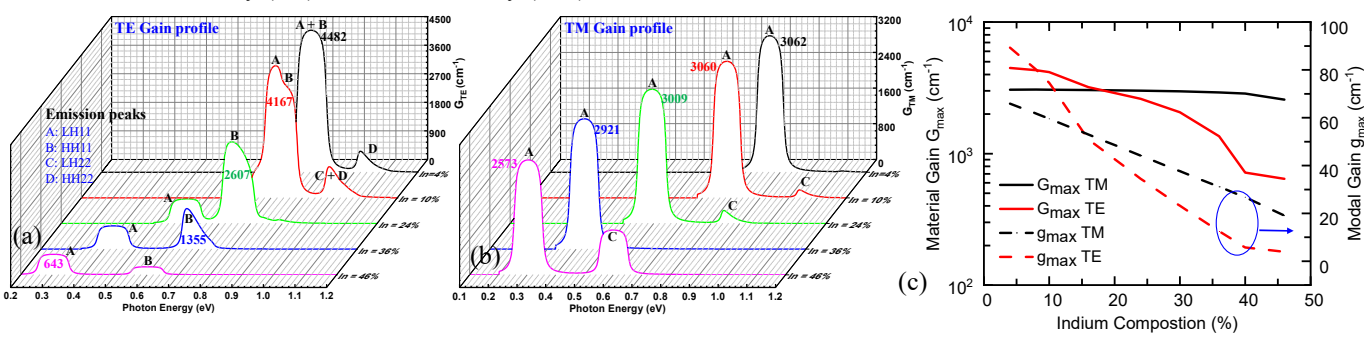


Fig. 5. The impact of In composition on the material gain spectrum of the 10 nm  $\epsilon$ -Ge QW laser for the (a) TE polarization and (b) TM polarization, for fixed biasing conditions. (c) The variation of  $G_{max}$  and  $g_{max}$  with the In composition in the In<sub>x</sub>Ga<sub>1-x</sub>As waveguide.

## A. Indium Composition in the Waveguide: Tensile Strain in Ge and its impact on the Gain Spectrum

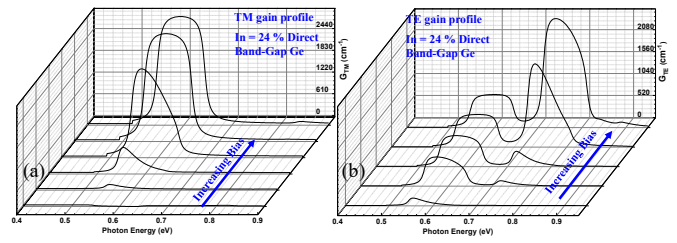


Fig. 6. Gradual increase in material gain with increasing current bias as population inversion occurs for direct bandgap Ge at In =24 % with (a) TM mode and (b) TE mode. The dependence of emission wavelength on the biasing condition is clear for the TE mode.

With an increase in In composition, the bandgap of  $In_xGa_{1-x}As$  reduces whereas the electron mobility and refractive index increases, impacting the total electrical and optical properties of the QW layer stack. The ground state eigen energies for electrons and holes in the  $\varepsilon$ -Ge QW are determined by the finite band offsets (*see*, Fig. 2) as well as the effective masses and band deformation, all of which are dependent on the tensile strain and consequently the In composition in  $In_xGa_{1-x}As$ .

The gain spectrum of the  $\varepsilon$ -Ge laser can be significantly tuned by altering the In composition in the In<sub>x</sub>Ga<sub>1-x</sub>As waveguide layer. Using the tunable cavity design discussed earlier (Section V.A), this variation of the gain spectrum for the TE and TM modes is shown in Fig. 5(a) and 5(b) for a 10 nm Ge OW, respectively. With an increase in In composition, the tensile strain in Ge increases, the LH-HH band degeneracy breaks, and the LH band moves upward, tending towards dominance. The material gain and the modal gain for the TE and TM modes are summarized as a function of In composition in Fig. 5(c). The TE gain depends strongly on the HH contributions as seen earlier through the transition matrix element, this causes the TE gain to drop with increasing In composition and can be seen through the TE polarization gain spectrum in Fig. 5(c). The A(j,n) term which accounts for the transition probabilities and the transition matrix element has a drastically different trend for the transitions from LH (nearly constant) and HH (decreasing) bands. The LH band transitions are always aligned with the bandgap of  $\varepsilon$ -Ge resulting in a nearly constant A(j, n) term, and correspondingly a constant gain profile for the TM mode is obtained. Interestingly, G<sub>TE</sub> as well as the TE mode peak wavelength is bias dependent, unlike the TM mode (see, Fig. 6a and b). At low bias, the LH band which is the dominant VB is excited easily and provides a gain peak. At higher bias (high current pumping), the quasi-fermi level separation is large enough to excite the LH as well as the HH band and a second peak of higher DOS, i.e., HH band can be seen. The TE gain is dependent strongly on the HH band emissions, which move to

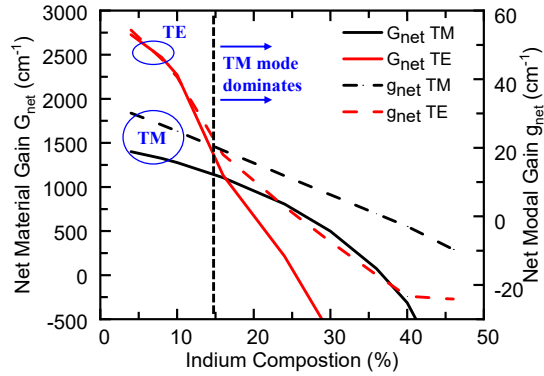


Fig. 8. Net material gain as a function of In composition: The transition point where Ge QW laser moves from a TE polarized laser to a TM polarized laser is identified at In = 15 % corresponding to a tensile strain of  $\sim$  1 %

increasingly higher energy separations as the tensile strain in Ge is increased resulting in the need for a significantly higher injection level to achieve lasing. It can also be observed that beyond In  $\sim$  40 %, the LH band transitions provide the TE gain peak as the contributions from the HH band to the TE gain have dropped significantly.

The maximum material gain G<sub>max</sub> as a function of injected charge density and total current density is shown in Fig. 7(a) and (b), respectively, for In = 4% (indirect bandgap Ge), In = 24 % (direct bandgap Ge) and In = 36 % (strongly direct bandgap Ge). At In = 24, 36 %, the  $G_{max}$  shown in Fig. 7(b) up to injected current levels of  $\sim 100 \text{ kA/cm}^2$  is due to the dominant VB, which is the LH band. A second jump in TE gain is observed at very high injection levels due to HH band transitions which are at a significantly larger energy separation than the dominant band-edge, i.e., LH band. The bias dependence of the emission peak for the TE mode is also seen in Fig. 6(b). To reach this second jump of TE gain, the In = 36% requires a much higher injected current density than the In = 24 % case, as the HH band is further away. Thus, for the TE mode, the peak energy (consequently  $\lambda_e$ ) varies drastically with applied bias and injection condition, as the G<sub>TE</sub> depends on LH and HH sub-band transitions. Such a jump and associated complications will not be possible for the TM mode as only the

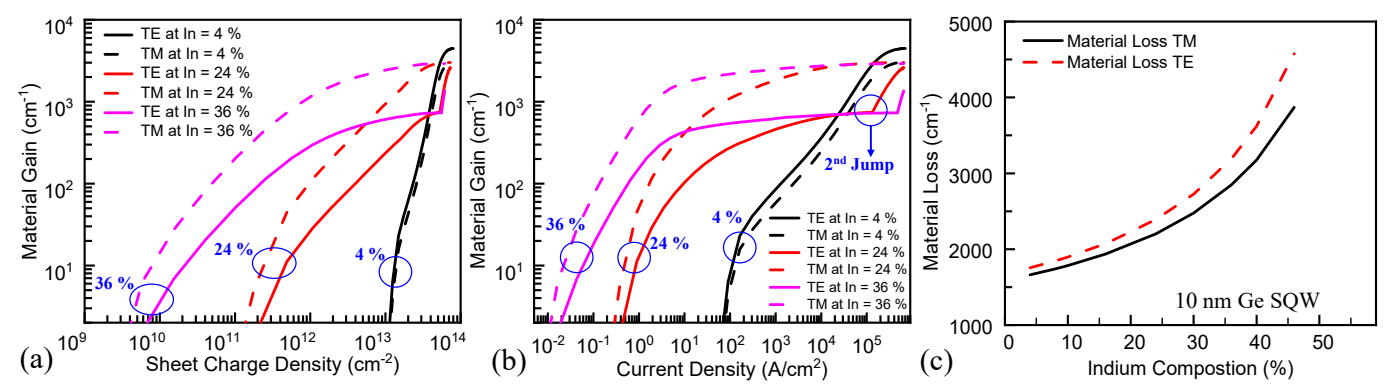


Fig. 7. In composition and tensile strain effect: Material gain of the Ge QW laser as a function of injected (a) sheet charge and (b) current density, at In = 4, 24 and 36 % for the TE and TM modes. (c) Impact of In composition in the  $\varepsilon$ -Ge/InGaAs single QW (SQW) cavity on the total material losses ( $\frac{\alpha_{tot}}{\Gamma_{ont}}$ ).

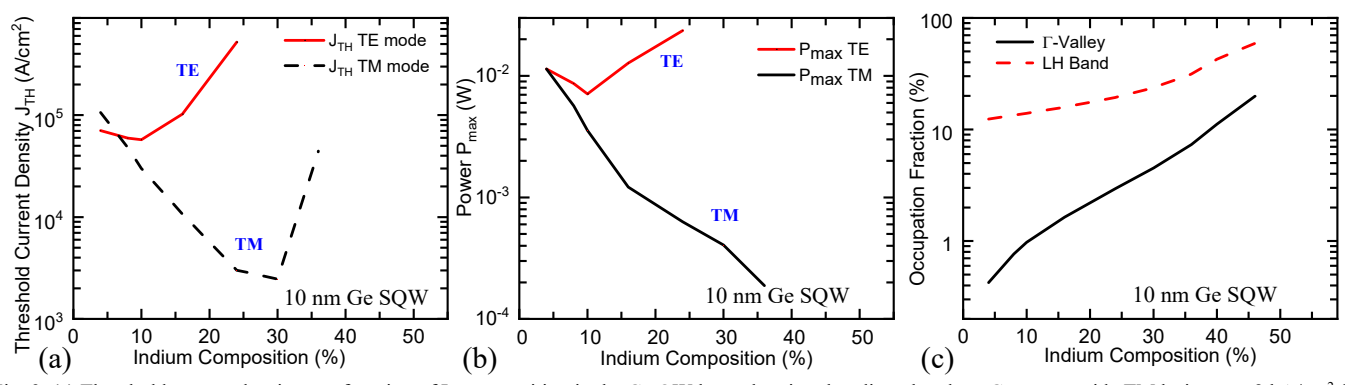


Fig. 9. (a) Threshold current density as a function of In composition in the Ge QW laser showing that direct bandgap Ge can provide TM lasing at  $\sim 2 \text{ kA/cm}^2$  for a 10 nm QW which is a significant improvement over existing Ge lasers. (b) Total power consumption by the entire SCH QW laser to achieve maximum gain beyond losses as a function of In composition. (c) Occupation fraction of the direct bands, i.e., LH valence and  $\Gamma$  conduction band as a function of In composition.

LH emissions contribute to the TM mode gain, resulting in an operating wavelength that is stable to bias variations.

From Fig. 7(a) and (b), it is also evident that the TE and TM modes provide similar gain and injection characteristics for low tensile strain configuration, i.e., In = 4 %. In this case, very high injection densities are needed to reach transparency and consequently lasing threshold. Thus, an unstrained/lowstrained Ge QW laser can provide comparable TE and TM gains at sufficiently high injection levels. To achieve lasing at lower injection densities, one must move to higher tensile strain, i.e., higher In composition which results in drastically different performance between the TE and TM modes as seen in Figs. 5-7, with TM mode lasing at lower injection levels and higher material gain. As one approaches higher In compositions three observations can be made: (i) low injection lasing is possible only from the TM mode, (ii) G<sub>TE</sub> reduces drastically whereas G<sub>TM</sub> remains nearly constant, and (iii) modal gain reduces monotonically due to decreasing  $\Gamma_{\text{opt}}$  (see, Fig. 4).

The TE mode experiences more material losses compared to the TM mode (see, Fig. 7c) due to the slight difference in the optical confinement factor due to a higher energy of emission attributed to the  $\Gamma$ -HH compared to  $\Gamma$ -LH emission resulting in a higher refractive index of InGaAs. The net material gain and modal gain beyond all losses are shown in Fig. 8. It is evident that the TM mode dominates at higher In compositions by providing a higher modal gain. The  $J_{TH}$  variation with In composition is shown in Fig. 9(a). At lower In compositions, the  $J_{TH}$  is high due to indirect bandgap Ge as the lasing medium resulting in a very small fraction of carriers occupying the  $\Gamma$ -

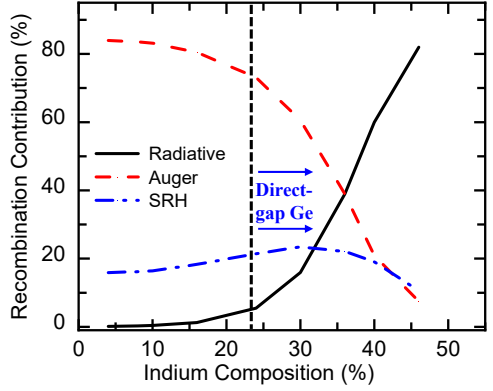


Fig. 10. Effect of In composition on relative contributions of different recombination mechanisms as Ge transitions to a direct bandgap material. The superior material quality ensures that the SRH recombination is minimal.

valley while majority of the carriers occupying the L-valley creating a high transparency current density (see Fig. 7b). The power consumption required to achieve the maximum gain beyond all losses is shown in Fig. 9(b). The  $J_{TH}$  can be reduced by increasing the tensile strain in Ge and thus increasing the  $\Gamma$ valley (and LH band) occupation fraction as shown in Fig. 9(c), but this also increases the material losses (inverse relation to confinement factor). Thus, the optimum J<sub>TH</sub> which can be attained considering the two competing mechanisms with increasing In composition: reducing confinement factor and increasing  $\Gamma$ -valley occupation, is  $\sim 2 \text{ kA/cm}^2$  at In  $\sim 30 \%$ . Beyond In  $\sim 36$  %, the material losses are too large to overcome in this cavity configuration, resulting in loss of lasing. This can also be seen in Fig. 8, where the net modal gain approaches zero. The tensile strain in Ge lowers the  $\Gamma$ -valley faster than the L-valley resulting in a gradual increase in carrier populations in the  $\Gamma$ -valley. As the  $\Gamma$ -valley lowers further with increasing In composition, the  $\varepsilon$ -Ge active layer starts to favor the direct radiative transitions resulting in an improved IQE.

The IQE quantifies the proportion of the radiative transitions compared to other non-radiative transitions such as SRH and Auger within the Ge active layer. The radiative, SRH, and Auger recombination contributions are dependent on the injection levels, band structure, minority carrier lifetime, doping and intrinsic carrier concentration, see Fig. 10. The IQE (see, Fig. 11) has improved at higher In composition due to the increase in radiative recombination within the active layer, but this improvement is limited by the Auger recombination which remains an issue for low bandgap materials such as Ge. The In composition (and corresponding tensile strain in Ge) can tune the emission peak over a wide range of wavelengths from 1.55

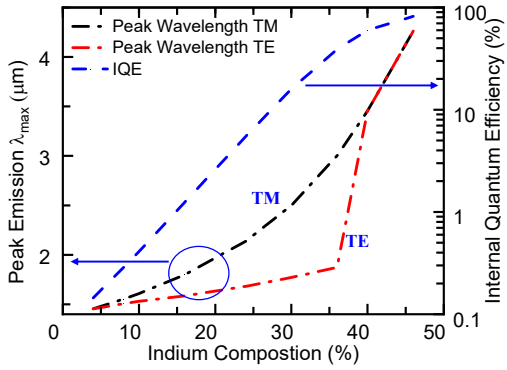


Fig. 11. The emission wavelength and IQE as a function of In composition for a 10 nm Ge QW.

 $\mu m$  to 4  $\mu m$  as seen in Fig. 11, thus showing potential for a wide range of applications. Beyond In = 40 %, the TE and TM emission peaks for maximum material gain are aligned as this

work, we study the QW thicknesses above 5 nm to limit the transition layers to within 20 % of the QW thickness.

Scaling the QW thickness is not expected to significantly

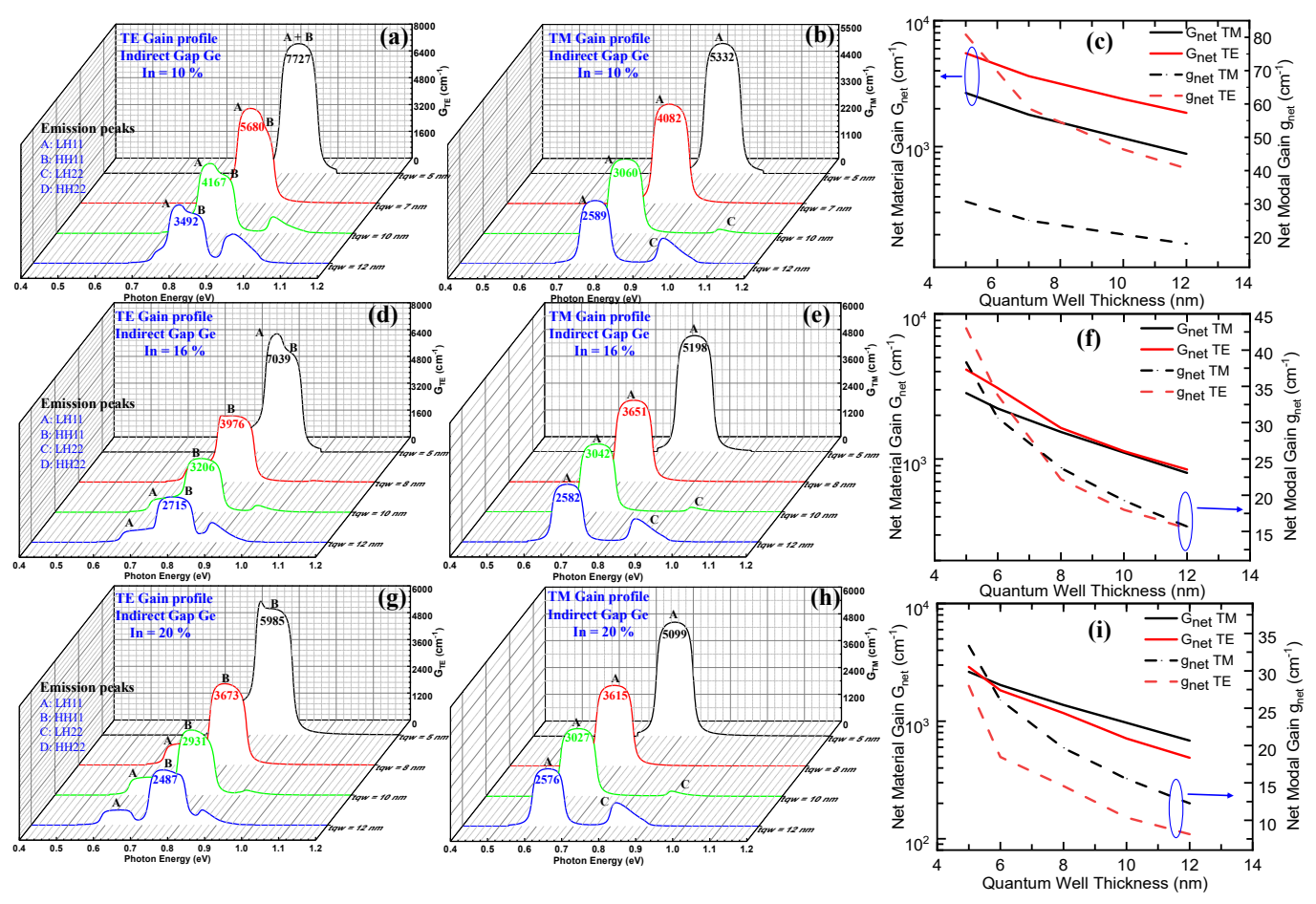


Fig. 12. The proposed Ge/InGaAs QW laser with indirect bandgap Ge as a function of QW thickness. Gain spectrum for the (a) TE and (b)TM mode for an In composition of 10 % with IQE  $\sim$  0.5 % and but with very high (c) net gains. Gain spectrum for the (d) TE and (e) TM mode for an In composition of 16 % with IQE  $\sim$  2 % and high (f) net gains. Gain spectrum for the (g) TE and (h) TM mode for an In composition of 20 % with IQE  $\sim$  4 % and high (i) net gains.

## emission is solely from the LH band.

Thus, the In composition impacts the losses, confinement, performance, and IQE of the  $\epsilon\text{-Ge/In}_x\text{Ga}_{1\text{-}x}\text{As}$  QW laser in a significant way, and the optimum choice of In composition is critical for lasing. Efficient laser performance comparable to direct bandgap lasers needs to be achieved while ensuring that the In composition in the structure is as low as possible due to the critical layer thickness of  $\epsilon\text{-Ge}$  QW layer and total thickness of the upper cladding layer.

#### B. Active Layer Design: Gain Spectra and QW Thickness

The Ge QW laser can provide good lasing and threshold performance over a wide range of emission wavelengths and In compositions, along with certain challenges and trade-offs. In this section, the impact of the QW thickness on the gain spectra is investigated. Due to the pseudomorphic growth of Ge on InGaAs, the strain-field creates a certain degree of roughness, interdiffusion, and non-ideality at the interface. Owing to the superior growth quality these non-idealities have been reduced to the lowest possible value of  $\sim 0.6$  nm [16] which indicates an ultra-abrupt interface with the precision of a single monolayer, consequently, this places a lower limit on the thickness of the Ge QW for reliable fabrication and operation. Thus, in this

affect the modal gain of a conventional OW laser due to the inverse trends between DOS and optical confinement [35]. Furthermore, the design of large wavelength configurations (large In composition) with maximum possible confinement factors is crucial. Following the tunable cavity design, the cavity is optimized at each configuration to achieve maximum confinement, as shown in Fig. 4. The impact of the QW thickness on the gain spectrum for the TE and TM polarization is shown in Fig. 12, at a fixed bias and low In compositions where Ge QW is still an indirect bandgap material. For In = 10% in Fig. 12(a-c), the  $\Gamma$ -HH transitions are still dominant over the  $\Gamma$ -LH transitions even though the LH band has risen significantly above the HH band as expected from Fig. 2. This phenomenon occurs due to two effects: (i) the significantly higher DOS of the HH band and (ii) the much lighter effective mass of holes in the LH band resulting in larger eigen energy and consequently reduced effective difference between the ground state energies of the HH and LH bands. For example, in Fig. 12(a) at  $t_{qw} = 5$  nm, the LH band ground state energy has risen nearly equal to the HH band ground state energy ( $E_{tr} \sim 0.9$ eV), resulting in an overlap of their respective gain peaks for the TE mode (note that although the peak locations are overlapping the gain contributions will be vastly different due

to the different DOS). This observation can be further verified through the  $G_{TE}$  peak location for  $t_{qw}=5$  nm in Fig. 12(b) which is also at  $\sim\!0.9$  eV, confirming that the LH and HH band ground states are nearly at the same energy in this configuration. As the  $t_{qw}$  is increased beyond 5 nm, the LH band ground state can be seen to move upwards resulting in distinguishable A:  $\lambda_{pk(\Gamma 1\text{-LH}1)}$ 

peak owing to the much larger DOS of the HH band. Here, at In = 16 %, the quantization effect, optical confinement, losses, broken degeneracy of LH and HH bands, and higher DOS of HH band, effectively cancel out the differentiating effects of each other resulting in nearly equal net material and net modal gains for the TE and TM polarizations (see, Fig. 12f). Moving

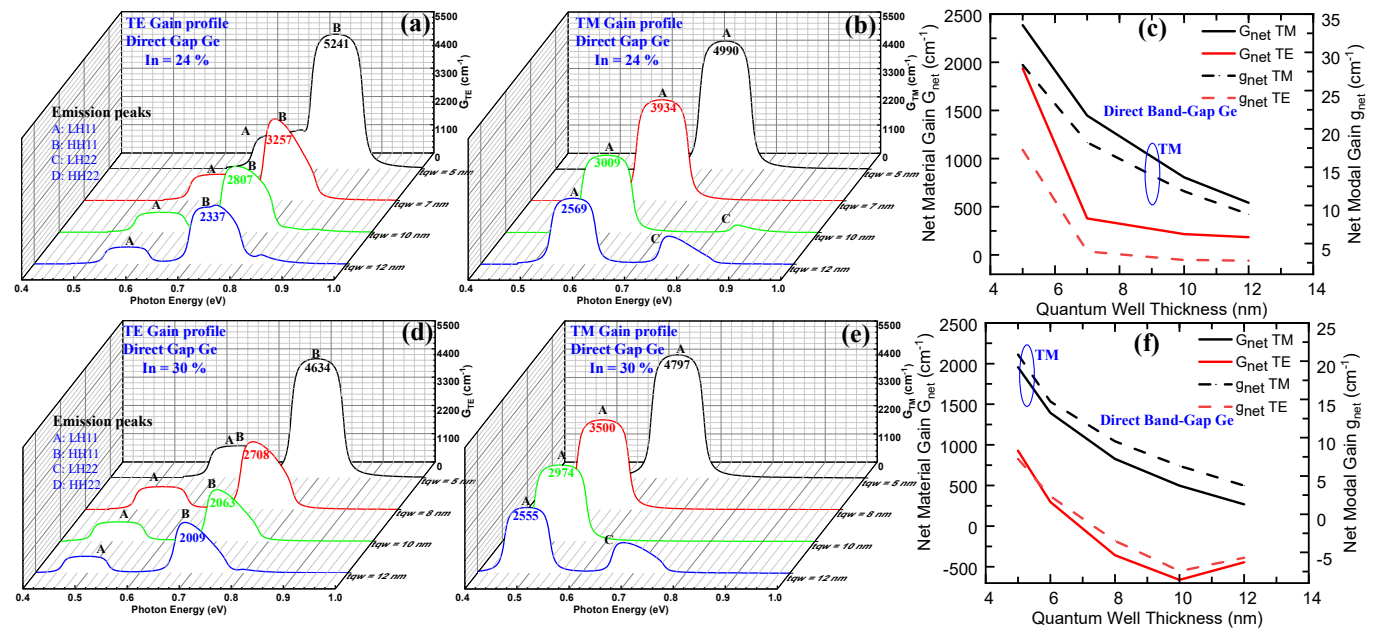


Fig. 13. Direct bandgap lasing from the proposed Ge/InGaAs QW laser for various QW thicknesses. Gain spectrum for the (a) TE and (b) TM mode for an In composition of 24 % with IQE  $\sim$  8 % and with moderate (c) net gains. Gain spectrum for the (d) TE and (e) TM mode for an In composition of 30 % with IQE  $\sim$  20 % and acceptable (f) net gains. Beyond In  $\sim$  36 %, the material gains cannot overcome the losses in SQW configuration for the Ge/InGaAs QW laser.

and B:  $\lambda_{pk(\Gamma_1-HH1)}$  peaks. Higher order excited state peaks C:  $\lambda_{pk(\Gamma_2-LH2)}$  and D:  $\lambda_{pk(\Gamma_2-HH2)}$  move farther away from the peak emissions as  $t_{qw}$  is reduced, and the probability of their excitation as well as the material gain associated with them drops exponentially. For the TM polarization, the contributions to the material gain arise only from the LH transitions thus, only A:  $\lambda_{pk(\Gamma_1-LH1)}$  and C:  $\lambda_{pk(\Gamma_2-L2)}$  are visible in the gain spectrum. As the thickness is increased to 12 nm and beyond, the quantization effects start to diminish and the higher-order peaks begin to merge creating a broad low-material gain spectrum.

The net material and net modal gain of the TE mode for indirect bandgap Ge at In = 10 % is summarized in Fig. 12(c) indicating that the TE mode will dominate the laser performance. Although a very high net modal gain for the TE mode can be achieved in this configuration, the expected IQE is  $\sim 0.5$  % and the J<sub>TH</sub> is expected to be  $\sim 100$  kA/cm<sup>2</sup>. As the QW thickness is reduced, the ground state eigen energy in the  $\Gamma$ -valley rises rapidly due to the low effective mass. The carriers can increasingly occupy the indirect L-valley, partially negating the effect of the tensile strain by lowering the transition probability and increasing the quasi-fermi separation required for transparency. At In = 16 %, the net modal and net material gains are nearly equal between the TE and TM modes as the QW thickness is varied, as seen in Fig. 12(d-f). Here, the spectrum has shifted to slightly lower energies compared to In = 10 % in Fig. 12(a) and (b) owing to the tensile strain. Furthermore, the LH band ground state is always visibly higher than the HH band ground state for all tqw (large LH and HH band separation) resulting in distinct peaks (see, Fig. 12d and e). The TE gain is contributed primarily from the B:  $\lambda_{pk(\Gamma_1-HH_1)}$ 

to In = 20 %, the Ge QW is nearly direct bandgap and an IQE of nearly 4% can be achieved in this configuration. Consequently, the TM gain dominates by providing the higher net modal gain, and the gain profiles for the TE and TM modes are shown in Fig. 12(g-i). One can note from Fig. 12, that the modal gain can be increased significantly by reducing the QW thickness owing to the tunable cavity design.

The gain spectra for the TE and TM modes for direct bandgap Ge at In = 24 % and In = 30 % are shown in Fig. 13(a-c) and Fig. 13(d-f) respectively. Due to the significant separation between the LH and HH bands, the dominant contributions to the TE and TM mode material gains are from the HH and LH valley respectively. The TM mode provides a higher material gain as well as net modal and net material gain as Ge is a direct bandgap material and LH band emissions are dominant. The In = 20 % SQW near-direct bandgap laser structure proposed in Fig. 12(g-i) can provide a TM net modal gain of  $\sim 20 \text{ cm}^{-1}$  for a reasonable  $t_{qw}$  of ~ 8 nm, at an IQE of 4%. Consequently, at In = 30 % using the direct bandgap Ge the net modal gain of 10  $cm^{\text{--}1}$  can be achieved at  $t_{qw}$  of  $\sim 8$  nm and 20  $cm^{\text{--}1}$  at  $t_{qw}$  of  $\sim 6$ nm, with an IQE of 20 %. The net material gain available in these QW structures is large and moving to MQW architectures can drastically scale the net modal gain. Beyond In  $\sim 36$  %, the modal gain cannot overcome the modal loss and the Ge SQW laser cannot lase (migrating to MQW or low-loss cavities is a potential solution).

## C. Active Layer Design: Threshold, Emission Wavelength and Quantum Well Thickness

For an ideal cavity of very low material loss, the  $J_{TH}$  will increase monotonically as  $t_{qw}$  is reduced due to the negative

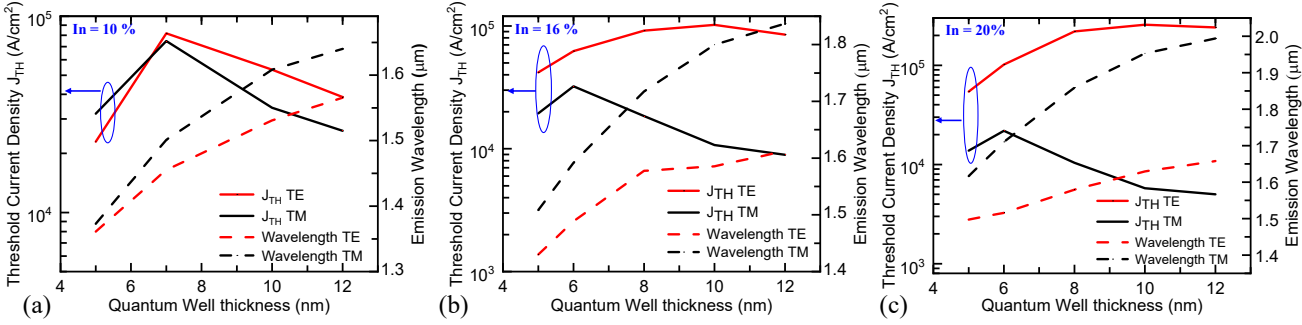


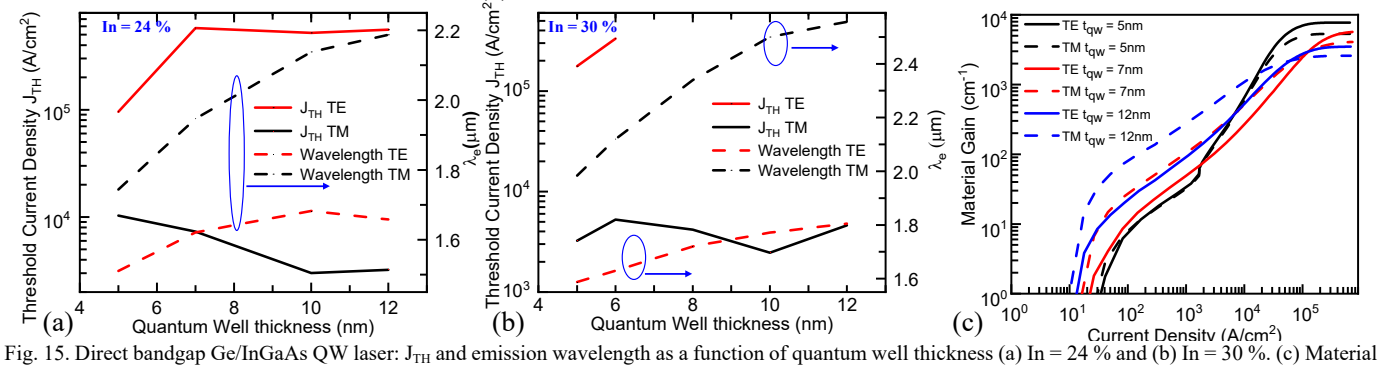
Fig. 14. Indirect bandgap Ge/InGaAs QW laser: J<sub>TH</sub> and emission wavelength as a function of QW thickness, (a) In = 10 %, (b) In = 16 % and (c) In = 20 %.

effect of the QW thickness scaling. As the quantum well thickness is reduced, the ground state eigen energies in the VB and CB increase, increasing the effective emission band edge. This results in an increase in emission energy and a consequent decrease in emission wavelength. The impact of QW thickness on J<sub>TH</sub> and emission wavelength for the TE and TM polarizations is shown in Fig. 14(a-c) for indirect bandgap Ge QW laser. At In = 16 % and beyond, the threshold current density for the TE mode lasing is significantly higher than the TM mode as seen in Fig. 14(b) and (c). Although the TE mode provides significant gain as seen in Fig. 12 and 13, the threshold current required for this gain is significantly higher than the TM mode. Thus, the Ge QW laser can operate with a good net material gain and a decent threshold current density only in the TM polarization. The impact of QW thickness on the J<sub>TH</sub> and emission wavelength for the TE and TM polarizations is shown in Fig. 15(a, b) for direct bandgap Ge QW laser at In = 24, 36%. The threshold current density can be reduced up to 2  $kA/cm^2$ , at In = 30 % for the TM polarization with an emission

doping in Ge of  $\sim 10^{18}$  cm<sup>-3</sup>. Thus, the results shown in this work assume a constant unintentional n-type doping of 10<sup>18</sup> cm<sup>-3</sup>.

#### VII. GE LASER DESIGN AND SURVEY

Lasing from indirect bandgap Ge has been a research endeavor for the past decade owing to the compatibility with Si technologies and emission ~ 1550 nm which is relevant for optical communication. The lower effective masses of Ge compared to GaAs and the pseudo-direct bandgap which is tunable using strain and alloying with Sn make it an attractive candidate for QW lasers. The challenge in achieving lasing from Ge is the dominant indirect L-valley which attracts large carrier populations but supports no radiative recombination, and techniques such as tensile strain and n-type doping have been suggested to lower the direct valley and achieve efficient lasing at lower threshold currents. One of the first reports for bulk Ge lasing included modeling the absorption spectra for heavily n-doped 200 nm thick Ge [26]. Using Ge with n-doping



gain of the Ge QW laser as a function of injected current density, at In = 10 %.

wavelength  $\sim 2~\mu m.$  The impact of  $t_{qw}$  scaling cannot be seen directly on the threshold trends as J<sub>TH</sub> is a strong function of the loss in the cavity (extracted from the G<sub>max</sub> v/s J curve) and the specific choice of mirror loss and FCA along with the confinement factor will cause the trend to differ drastically [36] (see, Fig. 15c).

### D. Active Layer Design: Doping

Ideally, the QW active layer should be intrinsic and free of impurities. However, during epitaxial growth, a finite density of unintentional n-type dopants is present, and the active layer will not be perfectly intrinsic. Consequently, the samples with which the band alignment (Fig. 2) and PCD minority carrier lifetime (Fig. 3) is calibrated, have an unintentional n-type

approaching ~10<sup>20</sup> cm<sup>-3</sup>, and a tensile strain of 0.25 % attributed to the thermal expansion coefficient difference between Ge and Si, Liu et. al., predicted that the threshold current could be lowered down to ~ 6 kA/cm<sup>2</sup> [26]. A similar approach of high doping and small tensile strain has been adopted in Ref. [37] to demonstrate the first lasing report from a Ge/Si cavity with a threshold current density approaching 300 kA/cm<sup>2</sup>. This approach has a few challenges; (i) the high n-type doping although helps raise the electron quasi-fermi energy closer to the direct band edge, results in aggravated Auger recombination, (ii) the material quality of Ge lasing media grown on Si substrate is defective due to the large lattice mismatch causing increased non-radiative recombination, (iii) considering the many-body effects, the band re-normalization at higher n-type doping can counter-act the fermi separation

advantage provided by the high doping [36,38], (iv) the cavity of a double heterostructure (DH) or QW needs to be Type I to provide confinement of carriers, the Si/Ge/SiGe system cannot provide this unless one relies on random defects at the interface to alter the band alignment [39]. Furthermore, it has been observed that the Ge-Si systems provide luminescence through indirect transitions between  $\Delta$ -valleys in Si and holes in Ge resulting in an inefficient radiative recombination [32]. Kurdi et. al., utilized a 30-band k·p calculation model to establish the material gain of ~ 3000 cm<sup>-1</sup> for FCA of 120 cm<sup>-1</sup> for bulk Ge with a tensile strain of 3 %. The optical transitions were neglected for the indirect L-valley, but the effect of the indirect valleys on the quasi-fermi energy movement and carrier conduction was considered [22]. Jiang et. al. predicted a gain of ~ 2000 cm<sup>-1</sup> for a 4 % uniaxial tensile strained Ge/SiGe QW system using 8 band k·p. It was noted that uniaxial tensile strain results in TE dominant gain, unlike the biaxial tensile case where the polarization is TM [40].

Ge 7 nm QW cavity design and gain analysis for a Type I system with a SiGeSn barrier was modeled using first-principles calculations for a tensile strain of 2.7 % [25] and 0.5 % [34]. At a tensile strain of 2.7 % (corresponding to In = 40 %), the Ge is a direct bandgap active region, and a significant density of carriers occupy the  $\Gamma$ -valley with the LH band being the dominant VB and hence the dominant mode is TM. This Ge-SiGeSn system has some key differences with the present work such as; only 1 LH bound state and no HH bound state, low band offset of 80-100 meV, and, a drastically higher refractive index of SiGeSn compared to InGaAs.

Another popular technique for making Ge transition to a direct bandgap material is alloying with Sn, with the transition occurring in the range Sn  $\sim$  7-10 % [36,41-43]. Chang *et. al.*, proposed a GeSn MQW with a SiGeSn cavity and used

compressive strain (upward movement of HH) to potentially reduce the J<sub>TH</sub> and make the dominant emission polarization TE. Furthermore, it was predicted that even when Ge is strongly direct bandgap at Sn = 16 %, the direct band occupation is nearly 12 % which is slightly higher than tensile Ge. The TE material gain of ~ 2500 cm<sup>-1</sup> was predicted at an emission wavelength of 2.8 μm, and the net modal gain for the 5-MQW structure was  $\sim 180 \text{ cm}^{-1}[41]$ . Fujisawa *et. al.*, used many-body theory (MBT) to circumvent the need for fitting parameters for broadening mechanisms generally associated with Fermi's Golden rule-based free carrier theory (FCT), to predict the lasing performance of MQW GeSn-SiGeSn Type I SCH system. The variation in spectral location and peak gain associated with the FCT as relaxation time is fitted can be avoided by using the MBT method. Peak material gain of ~ 3000 cm<sup>-1</sup> was predicted at an emission wavelength of 2.9 µm for a 10 nm QW and band offsets in the range of 50-100 meV [36]. Maczko et. al., utilized GeSn active layers and Ge barriers to form a OW laser structure with Type I alignment and band offsets in the range of 150 meV. The optimum Sn composition for forming the direct bandgap GeSn laser was determined to be 15 % where the emission is at  $\sim 2.48 \mu m$ . For narrow QW thickness as well as high Sn compositions, the material gain was seen to decrease because the carriers prefer to occupy L-valley in the Ge barrier rather than the GeSn direct valley, thus making thinner QWs unfavorable [43]. Dutt et. al., used the empirical pseudopotential method and the absorption spectra relation to estimate lasing performance from 300 nm bulk GeSn-on-Si DH cavity (Type II alignment). The high n-type doping requirement was reduced to  $\sim 10^{17}$  cm<sup>-3</sup> using the Sn alloying and achieving a material gain of  $\sim 1000$  cm<sup>-1</sup> while reducing the J<sub>TH</sub> to  $\sim 2.4$ kA/cm<sup>2</sup>, a number comparable to typical direct bandgap lasers. Unlike the tensile Ge case, the GeSn spectra has TE polarized emission due to the degenerate LH and HH bands [42]. Lasing

TABLE I : Benchmarking of the proposed monolithic ε-Ge/InGaAs SCH QW laser with electrically pumped Ge based lasers

Ref.	Lasing Material and Size	Type of Study	Technique	Cavity	Material Loss	JTH (kA/cm²)	Gain (cm <sup>-1</sup> )	Band Alignment	Band Offsets (c, v) in eV	Emission Wavelength (nm)	Temperature and polarization
26	Bulk Ge 200 nm	Theory	N-doping ~ 1e20, tensile Ge 0.25 %	Ge-Si	~ 500**	5.8	400*	Type II	-	1550	-
37	Bulk Ge 100 nm	Exp	n-doping ~ 1e20, tensile Ge 0.25 %	poly-Ge-Si	-	~ 280	-	Type II	-	1650	-
25	Ge SQW 7 nm	Theory	Strain balanced, Tensile Ge 2.7 %	Ge-SiGeSn QW	-	-	~ 2300#	Type I	~0.3,~ 0.1	~3100	300K, q-TM
34	Ge MQW 7 nm	Theory	Strain balanced, 5QW Tensile Ge 0.5 %	Ge-SiGeSn QW	~ 100- 1000	-	~ 3000#	Type I	~0.08,~0.06	1550	300K, q-TM
41	GeSn QW 10 nm	Theory	Strain balanced, Sn = 16 %, 5QW Compressive 0.5 %	GeSn- SiGeSn QW	~ 1000	~10##	~ 800#	Type I	~0.11, ~0.13	2883	300K, q-TE
43 ***	GeSn QW 8 - 14 nm	Theory	Sn = 10- 20 %, Compressive QW	GeSn- Ge QW	-	-	~ 1200	Type I	~0.17, ~0.16	~2580	300K, q-TE
40	Ge QW	Theory	Uniaxial tensile 4 %, N-doping 1e19	Ge-SiGe	400-600 **	-	~ 2000	Type I	~0.02,~0.12	~2210	300K, q-TE
22	Bulk Ge	Theory	High N-doping, tensile Ge 3 %	NA	120 **	-	~ 3000	-	-	~3000	80K
42	Bulk GeSn 300 nm	Theory	Moderate N-doping, Sn 0-10%	GeSn-Si	-	~2	~1200	Type II	-	~ 2500	-
32	Bulk Ge 350 nm	Theory	High N-doping, tensile Ge 0.25 %	Ge-SiGe	~517	~ 2-5	3000*	Type II	-	1550	-
38	Bulk Ge	Theory	Doping, MBT	NA	~ 200-800	~ 1- 10	~ 400	-	-	~1550	-
36	GeSn QW 10 nm	Theory	SCH compressive OW	GeSn- SiGeSn	~1000-2000	-	~3000	Type I		~ 2900	-
This work			`								
Ge QW In = 16 %	ε-Ge/InGaAs QW 10 nm	Theory	SCH QW tensile, tunable design cavity	Ge-InGaAs	1935	10.7	3042	Type I	0.38,0.28	1799	300K, q-TM
Ge QW In = 24 %	ε-Ge/InGaAs QW 10 nm	Theory	SCH QW tensile, tunable design cavity	Ge-InGaAs	2202	3	3009	Type I	0.22,0.35	2137	300K, q-TM
Ge QW In = 30 %	ε-Ge/InGaAs QW 10 nm	Theory	SCH QW tensile, tunable design cavity	Ge-InGaAs	2475	2.4	2974	Type I	0.2,0.4	2500	300K, q-TM

<sup>\*</sup> Net material gain, \*\* FCA, \*\*\* 12 nm QW with Sn = 15 %,  $N_{ini}$  = 6e18, #  $N_{ini}$  = 4e12, ## assuming efficiency of 75 %

from GeSn cavities was experimentally demonstrated by Wirths *et. al.*, using optical pumping and temperature-dependent PL measurements. The gain comparable to direct bandgap lasers of  $\sim 100~{\rm cm}^{-1}$  was achieved while a transition to direct bandgap GeSn was found to be  $\sim 9~\%$  and a lasing threshold of  $\sim 300~{\rm kW/cm}^2$ [44].

#### VIII. CONCLUSION

The merits of a novel biaxial tensile strained Ge OW laser in the wavelength range of 1.55 µm to 4 µm are analyzed using the proposed ε-Ge/In<sub>x</sub>Ga<sub>1-x</sub>As SCH architecture. The OW laser metrics are computed considering the electrical and optical phenomenon present within the ε-Ge laser structure through self-consistent physical solvers calibrated using in-house experimental results. The band alignment and minority carrier lifetime of the ε-Ge/In<sub>x</sub>Ga<sub>1-x</sub>As heterostructure are evaluated for various In compositions using x-ray photoelectron spectroscopy and photoconductive decay method, respectively. Key transitions in ε-Ge QW attributes are identified: (i) Ge transitions to a direct bandgap material at  $\varepsilon = 1.6 \%$  (In ~ 24 %), (ii) Ge QW transitions from type I to type II at In  $\sim 55$  %, and (iii) the transition to a TM mode dominant laser is identified at In  $\sim 15$  %. Using the tunable waveguide design strategy, the optical confinement is optimized. Different recombination mechanisms were analyzed as a function of strain in  $\varepsilon$ -Ge QW. The impact of QW thickness and In composition on the emission wavelength, polarization, IQE, J<sub>TH</sub>, and net gain is presented. This ε-Ge QW system can provide a net material gain of  $\sim 2000$  cm<sup>-1</sup> and a threshold current density of  $\sim 5$ kA/cm<sup>2</sup>, an improvement over existing Ge-based lasers.

#### IX. ACKNOWLEDGEMENT

The authors thank John K. Ghra (Systems Administrator for ECE, Virginia Tech) for assistance in computational services. S. J acknowledges that the views expressed herein do not necessarily represent the views of the U.S. Department of Energy or the United States Government.

### X. References

- H. Mahmudlu, et al., "Fully on-chip photonic turnkey quantum source for entangled qubit/qudit state generation", Nat. Photon., 2023, doi:10.1038/s41566-023-01193-1
- [2] M. K. Hudait, et al., "Design, Theoretical, and Experimental Investigation of Tensile-Strained Germanium Quantum-Well Laser Structure", ACS Appl. Electron. Mater., 3, 10, 4535–4547, 2021, doi: 10.1021/acsaelm.1c00660.
- [3] Sun, C., et al., "Single-chip microprocessor that communicates directly using light," Nature, vol. 528, no. 7583, pp. 534–538, Dec. 2015, doi: 10.1038/nature16454.
- [4] K. Tani, T. Okumura, K. Oda, M. Deura, and T. Ido, "On-chip optical interconnection using integrated germanium light emitters and photodetectors," *Opt. Express*, vol. 29, no. 18, pp. 28021-28036, Aug. 2021, doi: 10.1364/OE.432324.
- [5] R. Joshi, S. Karthikeyan and M. K. Hudait, "Monolithically Cointegrated Tensile Strained Germanium and InxGa1-xAs FinFETs for Tunable CMOS Logic," *IEEE Trans. on Electron Dev.*, vol. 69, no. 8, pp. 4175-4182, Aug. 2022, doi: 10.1109/TED.2022.3181112.
- [6] S.-K. Liao, et al., "Satellite-relayed intercontinental quantum network", Phys. Rev. Lett. 120, 030501, 2018, doi: 10.1103/PhysRevLett.120.030501.
- [7] S.-K. Liao, et al., "Long-distance free-space quantum key distribution in daylight towards inter-satellite communication", Nat. Photonics 11, 509– 513, 2017, doi: 10.1038/nphoton.2017.116.

- [8] D. J. Richardson, "Filling the light pipe", Science 330, 327–328, 2010, doi: 10.1126/science.1191708.
- [9] W. Cao, et al., "High-speed silicon modulators for the um wavelength band", Optica. 5, 1055–1062, 2018, doi: 10.1364/OPTICA.5.001055.
- [10] G. L. Mansell, et al., "Observation of squeezed light in the 2 μm region", Phys. Rev. Lett. 120, 203603, 2018, doi: 10.1103/PhysRevLett.120.203603.
- [11] Mancinelli, M, et al., "Mid-infrared coincidence measurements on twin photons at room temperature", Nat Comm., 8, 15184, 2017, doi:10.1038/ncomms15184.
- [12] Høgstedt, L. et al., "Low-noise mid-IR upconversion detector for improved IR-degenerate four-wave mixing gas sensing", Opt. Lett. 39, 5321–5324, 2014, doi: 10.1364/OL.39.005321.
- [13] A. Ghosh et al., "Growth structural and electrical properties of germanium-on-silicon heterostructure by molecular beam epitaxy", AIP Adv., vol. 7, no. 9, Sep. 2017, doi: 10.1063/1.4993446.
- [14] M. K. Hudait, et al., "High carrier lifetimes in epitaxial germanium-tin/Al(In)As heterostructures with variable tin composition", J. of Mat. Chemistry C 10: 10530-10540 (2022). doi: 10.1039/D2TC00830K.
- [15] D. Sukhdeo, et. al., "Impact of minority carrier lifetime on the performance of strained germanium light sources", Optics Comm, Vol. 364, pp 233-237, April 2016, doi: 10.1016/j.optcom.2015.11.060.
- [16] M. B. Clavel, et. al., "Multi-Valley Electron Conduction at the Indirect-Direct Crossover Point in Highly-Strained Germanium", *Phys. Rev. A*, 18: 064083-1-12 (2022), doi:10.1103/PhysRevApplied.18.064083.
- [17] R. People and J. C. Bean, "Calculation of critical layer thickness versus lattice mismatch for GexSi1-x/Si strained-layer heterostructures," *Appl. Phys. Lett.*, vol. 47, no. 3, pp. 322–324, Aug. 1985. doi: 10.1063/1.96206.
- [18] M. K. Hudait, Y. Zhu, N. Jain, and J. L. Hunter, Jr., "Structural, morphological, and band alignment properties of GaAs/Ge/GaAs heterostructures on (100), (110) and (111)A GaAs substrates", J. Vacuum Science & Technology B31: 011206, 2013, doi: 10.1116/1.4770070.
- [19] M. Clavel, D. Saladukha, P. Goley, T. J. Ochalski, F. Murphy-Armando, R. J. Bodnar, and M. K. Hudait, "Heterogeneously-Grown Tunable Tensile Strained Germanium on Silicon for Photonic Devices", ACS App. Mat. & Interfaces 7 (48):26470–26481,2015, doi: 10.1021/acsami.5b07385.
- [20] Y. Zhu, D. Maurya, S. Priya, and M. K. Hudait, "Tensile Strained Nanoscale Ge/In0.16Ga0.84As Heterostructure for Tunnel Field-Effect Transistor", ACS App. Mat. & Interfaces 6: 4947 4953, 2014, doi: 10.1021/am405988f.
- [21] M. Clavel, P. Goley, N. Jain, Y. Zhu, and M. K. Hudait, "Strain-Engineered Biaxial Tensile Epitaxial Germanium for High-Performance Ge/InGaAs Tunnel Field-Effect Transistors", *IEEE J. Electron Devices* Soc. 3 (3): 184-193, 2015, doi: 10.1109/JEDS.2015.2394743.
- [22] M. Kurdi, G. Fishman, S. Sauvage, and P. Boucaud, "Band structure and optical gain of tensile-strained germanium based on a 30 band k·p formalism" J. of App. Phys. 107, 013710 2010, doi: 10.1063/1.3279307.
- [23] TCAD Sentaurus Device Manual Release: T-2022.03, Synopsys Inc., Mountain View, CA, USA, 2022.
- [24] R. Joshi, S. Karthikeyan and M. K. Hudait, "Design Considerations and Quantum Confinement Effect in Monolithic ε-Ge/InxGa1-xAs Nanoscale FinFETs Down to N5 Node," *IEEE Trans. on Electron Dev.*, 2022, doi: 10.1109/TED.2022.3212337.
- [25] S. -W. Chang and S. L. Chuang, "Theory of Optical Gain of Ge-SixGeySn1-x-y Quantum-Well Lasers," *IEEE J. of Quantum Electronics*, vol. 43, no. 3, pp. 249-256, March 2007, doi: 10.1109/JQE.2006.890401.
- [26] J. Liu, et. al., "Tensile-strained, n-type Ge as a gain medium for monolithic laser integration on Si," Opt. Express 15, 2007, 11272-11277, doi: 10.1364/OE.15.011272
- [27] S. Johnston, et. al., "Simultaneous Measurement of Minority-Carrier Lifetime in Single-Crystal CdTe Using Three Transient Decay Techniques," *IEEE J. of Photov.*, vol. 4, no. 5, pp. 1295-1300, Sept. 2014, doi: 10.1109/JPHOTOV.2014.2339491.
- [28] L. A. Coldren, S. W. Corzine, M. L. Mašanović, Diode Lasers and Photonic Integrated Circuits, John Wiley & Sons, 2012.
- [29] S. L. Chuang, Physics of Photonic Devices, Second Edition, John Wiley & Sons, 2009.
- [30] Y. Arakawa and A. Yariv, "Theory of gain, modulation response, and spectral linewidth in AlGaAs quantum well lasers," *IEEE J. of Quantum Electronics*, vol. 21, no. 10, pp. 1666-1674, Oct 1985, doi: 10.1109/JQE.1985.1072555.

- [31] V. Swaminathan and A. T. MacRander, in Materials Aspects of GaAs and InP Based Structures, Prentice Hall, Englewood Cliffs, NJ, U.S., 1991, Ch. 1.
- [32] Y. Cai et al., "Analysis of Threshold Current Behavior for Bulk and Quantum-Well Germanium Laser Structures," IEEE J. of Sel. Topics in Quantum Electronics, vol. 19, no. 4, pp. 1901009-1901009, July-Aug. 2013, Art no. 1901009, doi: 10.1109/JSTQE.2013.2247573.
- [33] C. Lee, et al., "Direct-gap gain and optical absorption in germanium correlated to the density of photoexcited carriers, doping, and strain." Phys. Rev. lett., vol. 109,5 2012: 057402. doi:10.1103/PhysRevLett.109.057402.
- [34] Guo-En Chang, Shu-Wei Chang, and S. L. Chuang, "Theory for n-type doped, tensile-strained Ge-SixGeySn1-x-y quantum-well lasers at telecom wavelength," *Opt. Express* 17, 11246-11258, 2009, doi:10.1364/OE.17.011246.
- [35] J. Stohs, D. J. Bossert, D. J. Gallant and S. R. J. Brueck, "Gain, refractive index change, and linewidth enhancement factor in broad-area GaAs and InGaAs quantum-well lasers," *IEEE J. of Quantum Electronics*, vol. 37, no. 11, pp. 1449-1459, Nov. 2001, doi: 10.1109/3.958374.
- [36] T. Fujisawa and K. Saitoh, "Material Gain Analysis of GeSn/SiGeSn Quantum Wells for Mid-Infrared Si-Based Light Sources Based on Many-Body Theory," *IEEE J. of Quantum Electronics*, vol. 51, no. 5, pp. 1-8, May 2015, 7100108, doi: 10.1109/JQE.2015.2410283.
- [37] R. E. Camacho-Aguilera, et. al, "An electrically pumped germanium laser," Opt. Express 20, 11316-11320, 2012, doi:10.1364/OE.20.011316.
- [38] W. W. Chow, "Model for direct-transition gain in a Ge-on-Si laser" Appl. Phys. Lett. 7 May 2012; 100 (19): 191113. doi: 10.1063/1.4714540.
- [39] Y. Zhu, et. al, "Defect assistant band alignment transition from staggered to broken gap in mixed As/Sb tunnel field effect transistor heterostructure", J. App. Phys., 112: 094312, 2012, doi: 10.1063/1.4764880.
- [40] J. Jiang and J.Sun, "Theoretical analysis of optical gain in uniaxial tensile strained and n+-doped Ge/GeSi quantum well," *Opt. Express* 24, 14525-14537, 2016, doi: 10.1364/OE.24.014525.
- [41] G. -E. Chang, S. -W. Chang and S. L. Chuang, "Strain-Balanced GezSn1-z--SixGeySn1-x-y Multiple-Quantum-Well Lasers," *IEEE J.* of Quantum Electronics, vol. 46, no. 12, pp. 1813-1820, Dec. 2010, doi: 10.1109/JQE.2010.2059000.
- [42] B. Dutt et al., "Theoretical Analysis of GeSn Alloys as a Gain Medium for a Si-Compatible Laser," IEEE J. of Sel. Topics in Quantum Electronics, vol. 19, no. 5, pp. 1502706-1502706, Sept.-Oct. 2013, Art no. 1502706, doi: 10.1109/JSTQE.2013.2241397.
- [43] Maczko, H., Kudrawiec, R. and Gladysiewicz, M. "Material gain engineering in GeSn/Ge quantum wells integrated with an Si platform" Sci Rep 6, 34082, 2016, doi: 10.1038/srep34082.
- [44] Wirths, S., et al., "Lasing in direct-bandgap GeSn alloy grown on Si" Nature Photon 9, 88–92, 2015 doi: 10.1038/nphoton.2014.321.



Rutwik Joshi (Student Member, IEEE) received his Master's of Technology degree specializing in Microelectronics from the Indian Institute of Technology, Delhi, India, in 2019. He is currently working towards his Ph.D. degree in the Department of Electrical and Computer Engineering, Virginia Polytechnic Institute and State University, USA. He is a part of ADSEL Group at Virginia Tech working on

material and device research exploring Ge-based nanoscale quantum well lasers and transistors. Before joining Virginia Tech, he worked as an AMS engineer at Intel Corp specializing in device/circuit reliability CAD and EM/IR.



Steve Johnston received the B.S. degree in engineering from the Colorado School of Mines (CSM), Golden, CO, USA, in 1991; the M.S. degree in electrical engineering from the University of Illinois in Urbana-Champaign, Urbana, IL, USA, in 1995; and the Ph.D. degree in materials science from CSM in 1999. From 1991 to 1993, he was with Texas Instruments: an integrated-circuit manufacturer. Since 1996,

he has been with the National Renewable Energy Laboratory, Golden, CO, USA. His work and research interests have included minority-

carrier lifetime by photoconductive decay and time-resolved photoluminescence; deep-level transient spectroscopy; and imaging techniques that include photoluminescence, electroluminescence, and lock-in thermography.



Sengunthar Karthikeyan (S'19) received the Bachelor of Engineering degree in electronics and telecommunication engineering from Gujarat Technological University, Gujarat, India in 2013 and Master's of Technology degree in microelectronics and communication engineering from Indian Institute of Technology (Indian School of Mines) Dhanbad, Jharkhand, India in 2019. He is currently

pursuing the Ph.D. degree from the Bradley Department of Electrical and Computer Engineering. His current research interests include the design and MBE growth of IV/III-V heterostructure photodetector and laser structures, material characterization, device fabrication, and the heterogeneous integration of high mobility and low-power alternate channel devices for future transistor technology.



Mantu K. Hudait (M'08, SM'08) received the M.S. degree in materials science and engineering from IIT Kharagpur, Kharagpur, India, and the Ph.D. degree in materials science and engineering from Indian Institute of Science, Bangalore, India, in 1999. From 2000 to 2005, he was a Postdoctoral Researcher at

The Ohio State University and worked on the mixed cation and mixed anion metamorphic buffer, low bandgap thermophotovoltaics and heterogeneous integration of III-V solar cells on Si. From 2005 to 2009, he was a Senior Engineer in the Advanced Transistor and Nanotechnology Group at Intel Corporation. In 2009, he joined the Bradley Department of Electrical and Computer Engineering at Virginia Tech as an Associate Professor. He has over 195 technical publications and refereed conference proceedings and holds 60 US patents. His current research at Virginia Tech focuses on heterogeneous integration of compound semiconductors and GeSn on Si for photonics, quantum-well transistors, and photovoltaics. His research interests include III-V compound semiconductor epitaxy, metamorphic buffer and mixed As-Sb, mixed As-P based devices. He has received two Divisional Recognition Awards from Intel Corporation.



**Luke F. Lester,** an IEEE and SPIE Fellow, joined Virginia Tech in 2013 as the Head of the Bradley Department of Electrical and Computer Engineering (ECE) and was named the Roanoke Electric Steel Professor in 2016. Prior to joining VT, he was a professor of ECE at the University of New Mexico (UNM) from 1994 to 2013. Before joining UNM, Dr. Lester worked as an engineer for the General Electric Electronics

Laboratory in Syracuse, New York for 6 years where he co-invented the first Pseudomorphic HEMT, a device that was later highlighted in the Guinness Book of World Records as the fastest transistor. Later as a PhD student at Cornell, he researched and developed the first strained quantum well lasers that are now the industry standard for optical transmitters in data and telecommunications links. In 2001, he was a co-Founder and Chief Technology Officer of Zia Laser, Inc., a startup company using quantum dot laser technology to develop products for communications and computer/microprocessor applications. The company was later acquired by Innolume, GmbH. In 2012 he received the Harold E. Edgerton Award of the SPIE for his pioneering work on ultrafast quantum dot mode-locked lasers. He has published 148 journal articles and some 260 other publications. He was Editor-in-Chief of the IEEE Journal of Selected Topics in Quantum Electronics for 3 years from 2015-17.